

The manuscript has been accepted in *NeuroImage*.
A DOI will appear here once generated.

A Framework for Brain Atlases: Lessons from Seizure Dynamics

Andrew Y. Revell^{*,1,2,a}, Alexander B. Silva^{2,3,4,a}, T. Campbell Arnold^{2,3}, Joel M. Stein^{2,6}, Sandhitsu R. Das^{2,5}, Russell T. Shinohara^{7,8}, Dani S. Bassett^{1,2,3,5,10,11,12,13}, Brian Litt^{2,3,5}, and Kathryn A. Davis^{1,2,5}

¹Department of Neuroscience, Perelman School of Medicine, University of Pennsylvania, Philadelphia, PA 19104 USA

²Center for Neuroengineering and Therapeutics, University of Pennsylvania, Philadelphia, PA 19104 USA

³Department of Bioengineering, School of Engineering and Applied Science, University of Pennsylvania, Philadelphia, PA 19104 USA

⁴Medical Scientist Training Program, University of California, San Francisco, CA 94143 USA

⁵Department of Neurology, Perelman School of Medicine, University of Pennsylvania, Philadelphia, PA 19104 USA

⁶Department of Radiology, Perelman School of Medicine, University of Pennsylvania, Philadelphia, PA 19104 USA

⁷Department of Biostatistics, Epidemiology, and Informatics, Perelman School of Medicine, University of Pennsylvania, Philadelphia, PA 19104 USA

⁸Penn Statistics in Imaging and Visualization Endeavor, Perelman school of Medicine, University of Pennsylvania, PA 19104 USA

⁹Center for Biomedical Image Computing and Analytics, Perelman School of Medicine, University of Pennsylvania, PA 19104 USA

¹⁰Department of Electrical and Systems Engineering, School of Engineering and Applied Science, University of Pennsylvania, Philadelphia, PA 19104 USA

¹¹Department of Physics and Astronomy, College of Arts and Sciences, University of Pennsylvania, Philadelphia, PA 19104 USA

¹²Department of Psychiatry, Perelman School of Medicine, University of Pennsylvania, Philadelphia, PA 19104 USA

¹³Santa Fe Institute, Santa Fe, NM 87501

^aThese authors contributed equally

*Corresponding author: andrew.revell@pennmedicine.upenn.edu

1 **Brain maps, or atlases, are essential tools for studying brain function and organization. The abundance of available atlases used across the neuroscience literature, however, creates an implicit challenge that may alter the 2 hypotheses and predictions we make about neurological function and pathophysiology. Here, we demonstrate 3 how parcellation scale, shape, anatomical coverage, and other atlas features may impact our prediction of the 4 brain's function from its underlying structure. We show how network topology, structure-function correlation 5 (SFC), and the power to test specific hypotheses about epilepsy pathophysiology may change as a result of atlas 6 choice and atlas features. Through the lens of our disease system, we propose a general framework and algo- 7 rithm for atlas selection. This framework aims to maximize the descriptive, explanatory, and predictive validity 8 of an atlas. Broadly, our framework strives to provide empirical guidance to neuroscience research utilizing the 9 various atlases published over the last century.**

Brain Atlas | Networks | Epilepsy | Structure-function

1 Introduction

2 How we define anatomical brain structures and relate those 3 structures to the brain's function can either constrain or en- 4 hance our understanding of behavior and neurological dis- 5 eases^{1–4}. Discoveries by scientists like Carl Wernicke and 6 Pierre Paul Broca, who mapped specific brain regions to speech 7 function, in addition to case studies from Phineas Gage and 8 H.M., who lost specific brain regions with resultant changes 9 in brain function and behavior, exemplify how brain structure 10 and function are fundamentally linked^{5–7}. Properly labeling 11 brain structures is paramount for enabling scientists to ef- 12 fectively communicate about the variability between healthy 13 individuals and about the regions involved in neurological 14 disorders⁸. Yet, no consensus has been reached on the most 15 appropriate ways to label and delineate these regions, as ev- 16 ident by the wide variety of brain maps, or atlases, defining 17 neuroanatomical structures⁹.

18 In common usage, an atlas refers to a “collection of maps”¹⁰ 19 that typically defines geo-political boundaries and may include 20 coarse borders (continental), fine borders (city), and anything 21 in between (country; **Fig. 1a**, left). Borders¹¹ are usually con- 22 sistent across atlases of the world. In contrast, atlases of the 23 brain are not consistent. Four separate atlases (**Fig. 1a**, right) 24 may define the superior temporal gyrus differently. For ex- 25 ample, approximately ninety percent of the *anterior* superior 26 temporal gyrus in the Harvard-Oxford atlas¹⁶ overlaps with 27 the *posterior* superior temporal gyrus in the Hammersmith

28 atlas¹⁷. Atlases may also differ in other ways, including parcel- 29 lation size, neuroanatomical coverage, and complexity of brain 30 region shapes. For instance, the Yeo atlas¹⁸ contains 7 or 17 31 parcels while the Schaefer atlases¹⁹ may have between 100 32 and 1,000 parcels. Complicating matters further, atlases can 33 differ in their intended use. The MMP atlas²⁰ was intended 34 for surface-based analyses²¹, yet a volumetric version (without 35 subcortical structures) was independently created and used in 36 connectivity studies²². The plethora of available atlases poses 37 a problem for reproducibility in studying healthy and diseased 38 populations and for metanalyses describing the involvement 39 of different regions of the brain in various diseases. This has 40 been termed the *Atlas Concordance Problem*⁴.

41 In the present study, we perform an extensive evaluation of 42 the available atlases in the neuroscience literature (**Table 1**) by 43 examining the effect of varying features such as parcellation 44 size, coverage, and shape (**Fig. 1b**) on structural connectivity 45 (**Fig. 1c**). We also examine how atlas choice changes structural 46 network topology by measuring structure-function correlation 47 (SFC) using an atlas-independent measure of functional connec- 48 tivity (**Fig. 1d**). We utilize a total of 55 brain atlases, including 49 many routinely used in common neuroimaging software. Note 50 the important distinction between the terms atlas, template, 51 and stereotactic space⁹ (see **Fig. S1**). We found that different 52 atlases may alter the *power* to test a hypothesis about epilepsy 53 pathophysiology that seizures propagate through the underly- 54 ing structural connections of the brain. This hypothesis has 55 been previously supported in prior research^{13,14,23,24}.

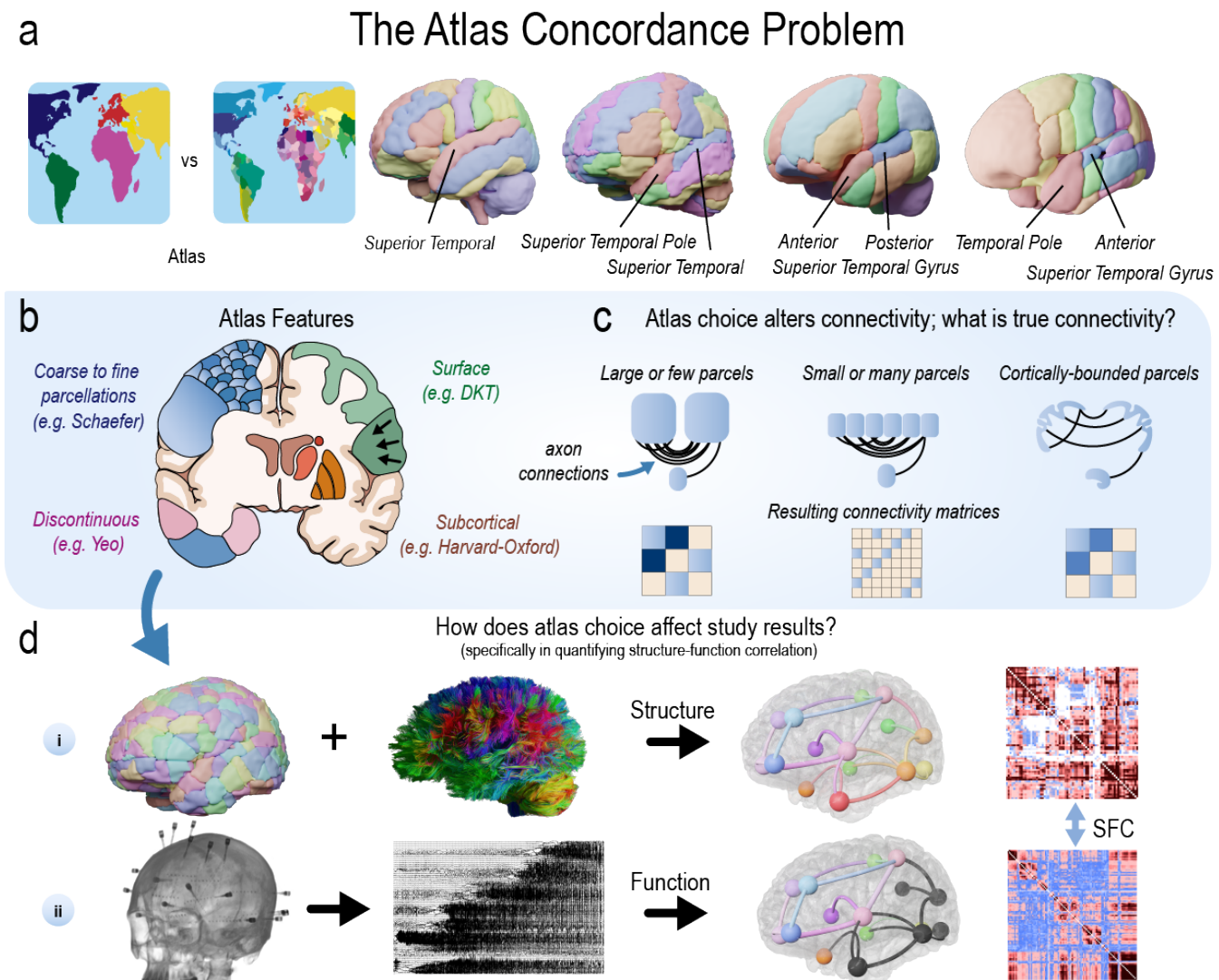


Fig. 1. Many brain atlases are available in the neuroscience literature. | **a**, In common usage, an atlas refers to a “collection of maps”¹⁰ that defines geo-political borders at different scales. Although borders¹¹ are usually consistent across atlases of the world, they are typically not consistent across atlases of the brain. Four separate atlases (left-to-right: Cerebra, AAL, Hammersmith, Harvard-Oxford) may define the superior temporal gyrus differently. The lack of consistency across these labels poses a problem for reproducibility in cognitive, systems, developmental, and clinical studies, as well as metaanalyses describing the involvement of different regions of the brain in various diseases⁴. This challenge has been previously referred to as the Atlas Concordance Problem. **b**, Atlases can have varying features (see also Table 1). **c**, Thus, all current connectivity studies in neuroscience may not accurately reflect some fundamentally “true” architecture. For example, atlases with either large or small parcels may affect the structural connectivity matrices that are used to define the “true” network architecture of the brain, and subsequently that are used to test hypotheses or make predictions about the brain. **d**, When combined with white matter tracts reconstructed from diffusion MRI, atlases can be used to measure how different regions of the brain are structurally connected (i). Similarly, intracranial EEG (iEEG) implants can record neural activity to measure how different regions of the brain are functionally connected (ii). Technologies such as fMRI, MEG, and many others can also measure functional connectivity. The statistical similarity between structural and functional connectivity measurements can be calculated (e.g., structure-function correlation; SFC). Such estimates have been used to better understand the pathophysiology of disease. In this study, we evaluate how the varying atlases may alter the power to test a specific hypothesis about the brain’s structure-function relationship in epilepsy.

56 In the context of our experimental design, we propose a
 57 new framework outlining how to appropriately choose an atlas
 58 when designing a neuroscience experiment. This framework is

59 derived from historical foundations for assessing the validity
 60 and effectiveness of animal models²⁵, network models²⁶, and
 61 psychometric tests²⁷, which try to maximize the (1) descrip-

Please see the end of this document for a high-resolution, highlightable version

Atlas [regions]	Sources	3D Render	Description	Variations
AAL [116;120;166]	1-7 SPM	S	Structural atlas. Manual identification using a defined labeling protocol on single subject template (Collin-27). Three versions: Version 2: updated boundaries. Version 3: further parcellations. Successor to Talairach.	AAL: AAL1, AAL2, AAL3, AAL600, AAL-JHU AAL1 AAL2 AAL3 AAL600
AICHA [384]	8	F	Functional atlas based on rsfMRI; 281 subjects. Each ROI has (1) homogeneity in its functional activity (2) a homotopic contralateral counterpart with which it has maximal connectivity.	
Brainnetome [246]	9-10 DSstudio	S	Connectivity-based parcellation. Based on idea that clustered regions of a brain region should share similar connectivity profiles; 40 subjects from HCP dataset. 210 cortical, 36 subcortical.	
Brodmann [48]	11-13 MRIcron	S	Developed by independent group at Washington University in St. Louis. Published with MRIcron software. Warned by developer to be used with caution - not validated, nor based on multiple individuals.	
CerebrA [102]	14	S	Structural atlas. Non-linear registration of cortical and subcortical labeling from Mindboggle-101 dataset (see DKT below) to the symmetric MNI-ICBM2009c template, followed by manual editing.	Craddock: N parcellations N=200 N=400 1.7 cm 1.0 cm DKT surface DKT surface DKT volumetric
Craddock [N]	15-17	F	Functional atlas; rsfMRI; 41 subjects. ROIs are spatially clustered into regions of homogeneous functional connectivity. May be N regions. 200/400 regions publicly available. 4x4x4 mm ³ resolution fMRI. Resliced.	
DKT [109]	18-23 FreeSurfer	S	DKT is a labelling protocol. DK is old protocol. Used on Mindboggle-101 dataset (101 brains). Probabilistic atlas using joint fusion algorithm. Surface version in FreeSurfer (40 brains). Volumetric version, 20 brain subset. Non-cortical: Neuromorphometrics BrainCOLOR atlas (aseg).	DKT: Surface (probabilistic labeling of individual with surface-based registration), Volumetric (labeling with volumetric-registration)
Destrieux [189]	24-25 FreeSurfer	S	Probabilistic atlas of surface anatomy created from: (1) Manual labeling, (2) surface geometry, (3) spatial relationship of neighboring structures. Available in FreeSurfer with subcortical structures added.	Harvard-Oxford: Cortical/subcortical only, combined, symmetric, nonsymmetric Symmetric Nonsymmetric Subcortical Combined Cortical + Subcortical
Gordon-Petersen [333]	26-27	F	Identification of abrupt transitions in resting-state functional connectivity to identify parcellations. Based on rsfMRI. 108 subjects. Intended for surface-based analyses.	
Hammersmith [83]	28-30	S	Manually identified 83 structures using defined labelling protocol; 30 subjects. Maximum probability map. First version in 2003 with 49 structures. Named after London hospital, Hammersmith. Hammers is author.	
Harvard-Oxford [48 + 21]	31-32 FSL	S	Manual segmentation using defined labelling protocol; 37 subjects. Cortical and subcortical atlases provided separately. Left and right structures have same labels (symmetry). Must preprocess.	
JHU [48; 20]	33-35 FSL	S	White matter atlas. Two versions. (1) Labels: Hand segmentation average of diffusion MRI; 81 subjects. (2) Tracts: probabilistic identification from deterministic tractography; 28 subjects.	JHU: Labels, tracts Labels Tracts
Julich [121]	36-37 FSL	S	Cytoarchitecture atlas. Successor to Brodmann. Average of 10-subject post-mortem cyto- and myelo-architectonic segmentations. Update to the Eickhoff SPM Anatomy Toolbox v1.5. Whole brain is not covered.	
MMP [380]	38-40 DSstudio	M	Multi-modal parcellation: (1) Architecture - T1w/T2w myelin maps + cortical thickness, (2) function - task-fMRI, (3) connectivity, (4) topography. 210 subjects. Cortical ONLY. Originally intended for surface analysis. Volumetric version independently created and used.	Random: N parcellations, cortical, whole-brain, subparcellated N=30 N=100 N=1,000 N=10,000 N=10 lemon 5 cm grape 2 cm pea 1 cm
Random [N]	41-42	V	Brain is randomly parcellated into N regions. Variations used in studies include cortical and whole-brain. Other atlases (e.g. AAL) and their regions may be further randomly divided, or subparcellated.	
MNI Structural [9]	43 FSL	S	9 regions, including lobar and some subcortical regions. Hand segmented 50 subjects. Transformed into MNI152 space, averaged, probability maps produced. 25% max probability is shown.	Schaefer: 100 to 1,000 parcellations (by 100), named to Yeo 7 and 17 N=100 N=500 N=1,000
Schaefer [100-1000]	44-45 GitHub	F	Based on rsfMRI. Clusters found with gradient-weighted Markov Random Field model. 1489 subjects. Cortical only. Spatial resolutions provided: 100 - 1000 parcellations (by 100). Well documented.	
Talairach [1105]	46-50 FSL	S	Conversion of original Talairach labeling. Digitized version of the original (coarsely sliced) Talairach atlas and registration to MNI 152 space. Atlas provided in FSL.	Yeo: 7/17 parcellations; Cortically bounded or liberal Cortically bounded liberal discontinuous
Yeo [7; 17]	51-52 FreeSurfer	F	1000 subjects; rsfMRI. Clustered cortical regions by pattern of functional connectivity. Results in non-spatially continuous clusters. 7 and 17 clusters based on stability of clustering algorithm.	
Region-specific	53-56 FSL	V	Atlases created for specific regions, usually high quality + high degree of accuracy (e.g. post-mortem histological verification). Examples: Thalamus nuclei, hippocampus, and other specific structures.	Thalamus, Hippocampus, Cerebellum Cerebellum
Population-specific	57-58	V	Atlases created from a specific population (e.g. elderly, pediatric, non-human). Disease-specific defines regions specific for disease (e.g. MS lesion probabilistic locations).	Pediatric, Elderly, Disease specific Neonatal M-CRIB (Melbourne)

Table 1. Atlases. | Atlas sources are detailed in Table S1 and abbreviations are in the glossary. **S:** Structurally defined atlas; **F:** Functionally defined atlas; **M:** Multi-modally defined atlas; **V:** A variably defined atlas that may be structurally, functionally, or multi-modally defined; **ROI:** region of interest; **HCP:** Human connectome project dataset ¹²; **MS:** multiple sclerosis.

62 tive, (2) explanatory, and (3) predictive validity ²⁶ of a model.
63 Atlases are a *tool* for investigators to test for causality and
64 to make predictions about the brain. Thus, this framework

65 incorporates a short discussion on explanatory modeling and
66 predictive modeling, each with different goals ("To Explain or
67 to Predict?" ¹⁵). A one-size-fits-all approach may not exist for

Atlas Morphology: Sizes and Shapes

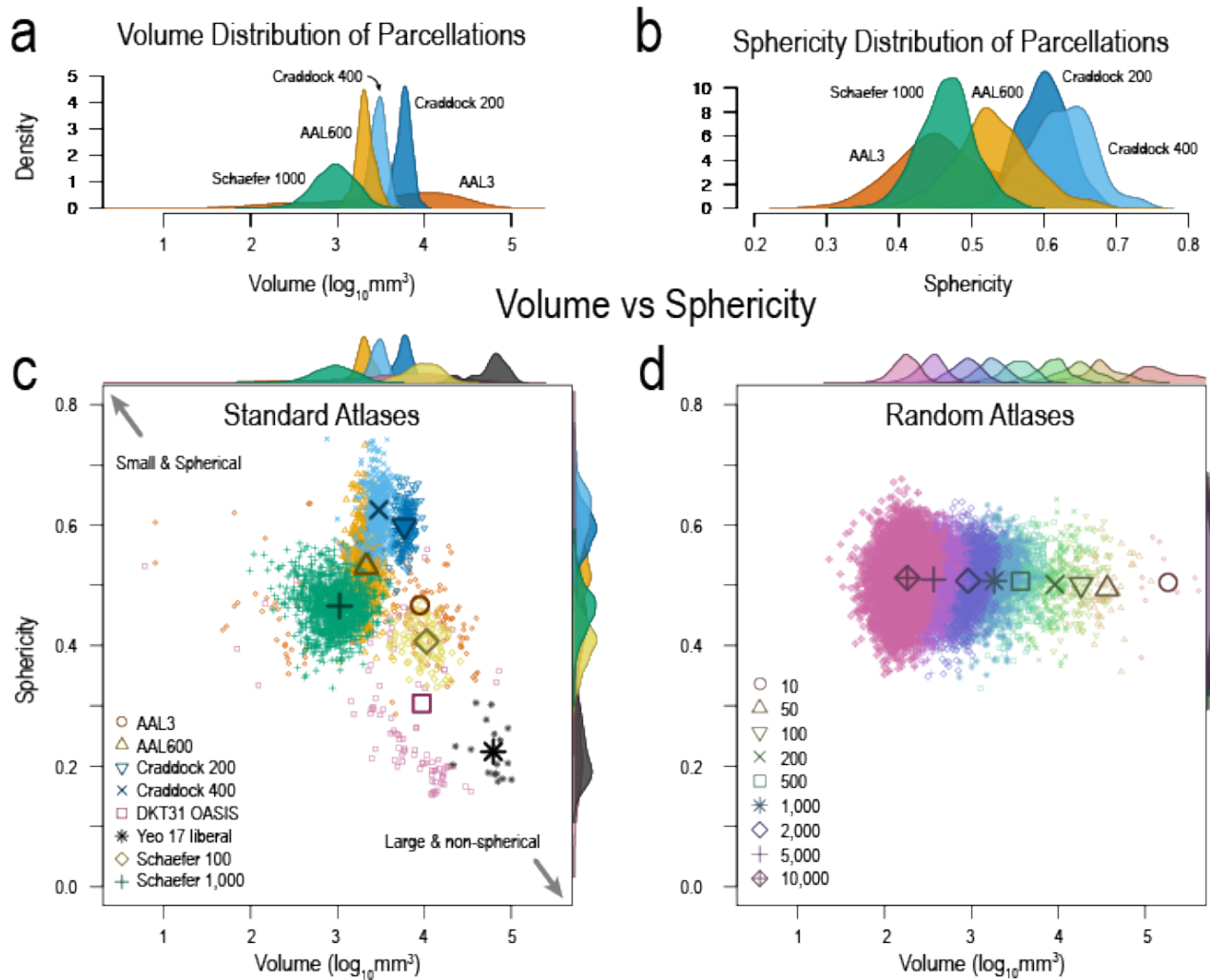


Fig. 2. Atlas morphology: sizes and shapes. **a**, Volume distribution of atlas parcellations demonstrating the diversity of parcellation sizes. **b**, Parcellation sphericity distributions illustrating how the shapes of different parcellations may not be uniform. **c**, Volumes versus sphericity showing how some atlas parcellations may be small and spherical, while others may be large and non-spherical. This illustrates the non-uniformity in atlas parcellations. **d**, Volumes and sphericity of random atlases showing the uniformity of sphericity with changing volumes. Random atlases allow us to study (1) the effect of parcellation scale without the confound of shape effects and (2) the need for accurate anatomical boundaries to test a hypothesis about the structure-function relationship in the brain at seizure onset. Numbers in legend represent the number of parcellations for each random atlas. Remaining atlases are in [Fig. S2](#).

68 selecting an atlas, nor should it²⁸; while there is one Planet
 69 Earth with a single atlas for a particular use (e.g., an atlas
 70 of the geo-political borders for a given point in time), there
 71 are many brains, with anatomical and functional variability
 72 across populations and species²⁸. We hope our framework
 73 provides empirical guidance to neuroscience research utilizing
 74 the various atlases published over the last century.

75 Results

76 **Clinical Data.** Forty-one individuals (mean age 34 ± 11 ; 16
 77 female) underwent High Angular Resolution Diffusion Imaging

78 (HARDI), composed of thirteen controls (mean age 35 ± 13 ;
 79 6 female) and twenty-eight drug-resistant epilepsy patients
 80 (mean age 34 ± 11 ; 12 female) evaluated for surgical treatment.
 81 Of the twenty-eight patients, twenty-four were implanted with
 82 stereoelectroencephalography (SEEG) and four with electro-
 83 corticography (ECOG). Ten SEEG patients (mean age 34 ± 8 ;
 84 4 female) had clinical seizure annotations, and the first seizure
 85 from each patient (mean duration 81s) without artifacts was
 86 selected for SFC analyses. Patient and control demographics
 87 are included in [Table S2](#).

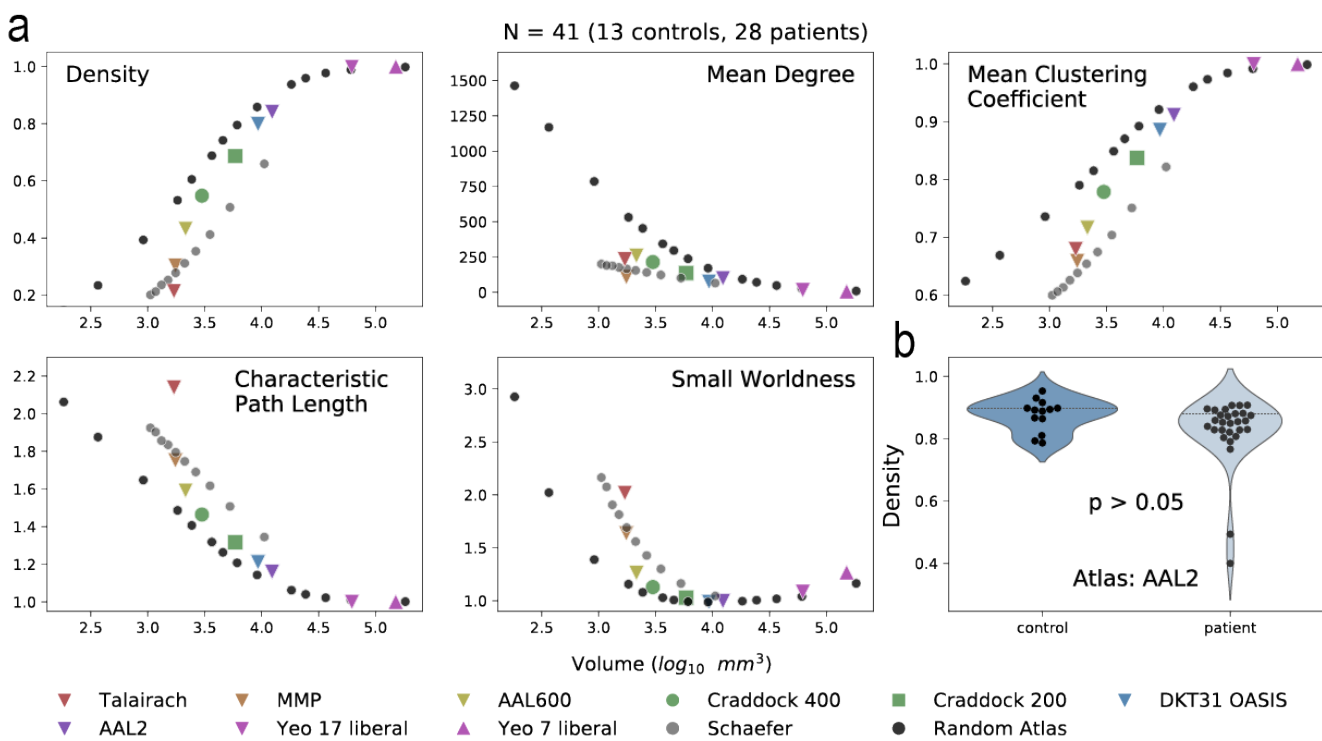


Fig. 3. Structural network differences between atlases. | a, Density, mean degree, mean clustering coefficient, characteristic path length, and small worldness were calculated for structural connectivity networks. A subset of atlases is shown. Remaining atlases studied are shown in Fig. S3. The average parcellation volume was calculated for each atlas and the corresponding network measure was graphed as the mean of all subjects (N=41; 13 controls, 28 patients). b, Controls and patients were not significantly different in density for the AAL2 atlas (Mann-Whitney U test), illustrating that global structural network measures are similar between cohorts. However, specific edge-level connections between cohorts may be different, and characterizing these differences is out of the scope of this manuscript. Controls and patients were separated and shown in Fig. S4. Network measures using different threshold are shown in Fig. S5.

88 **Atlas Morphology: Sizes and Shapes.** We hypothesized that 111
 89 atlas morphological properties, including size and shape 112
 90 (Fig 2), affect SFC. To test this hypothesis, we first quantified 113
 91 the distributions of parcellation sizes (Fig 2a) and shapes 114
 92 (Fig 2b) in various atlases. These results exemplify the 115
 93 diversity of atlas parcellation morphology. Fig 2c shows a 116
 94 comparison of individual parcellation volumes and sphericities. The 117
 95 remaining atlases are shown in Fig. S2. In contrast to standard 118
 96 atlases, random atlases have constant sphericity with respect 119
 97 to volume size. Note that the distribution of parcellation 120
 98 shapes (i.e. sphericity) is similar across parcellation sizes in 121
 99 random atlases and their parcellations may not represent true 122
 100 anatomical or functional boundaries. Thus, random atlases 123
 101 allow us to study how parcellation scale affects network structure 124
 102 and SFC while keeping the effect of shape constant. Crucially, 125
 103 random atlases also allow us to explore if accurate and 126
 104 precise anatomical boundaries are essential in some experimental 127
 105 designs²⁹.

106 **Varying atlases affect structural network topology.** Although 128
 107 the morphology of atlas parcellations is diverse, we aimed to 129
 108 investigate how these morphological characteristics (partic- 130
 109 ularly parcellation scale) affect structural network topology 131
 110 (Fig. 3). Networks are the basis upon which we compute SFC, 132
 111

112 and not necessarily morphological characteristics, therefore, 113 we measured how network density, mean degree, characteristic 114 path length, mean clustering coefficient, and small worldness 115 change as a function of parcellation scale (Fig. 3a). We found 116 that the change in these network measures are congruent 117 between standard and random atlases and previous studies³⁰. 118 We also show that mean density, a global network measure, 119 is similar between our control (N=13) and patient (N=28) 120 cohorts (Fig. 3b).

121 **Varying atlases affect SFC: single subject.** Fig. 4 illustrates 122 an overview of how SFC is calculated. Structure is measured 123 with high angular resolution diffusion imaging (HARDI) and 124 function is measured with SEEG electrode contacts. Structural 125 connectivity matrices are generated based on the atlas chosen 126 (Fig. 4a) and functional connectivity matrices are generated 127 based on broadband (1 – 127 Hz) cross-correlation of neural 128 activity between the electrode contacts in windows of time 129 (Fig. 4b, see Methods section on "Functional Connectivity 130 Network Generation"). Thus, the structural network is static 131 while the functional network is computed across time. The 132 connectivity matrices shown are example data from a single 133 patient, sub-patient07. Functional connectivity matrices are 134 shown for 6 hours before seizure onset, 90 seconds before 135

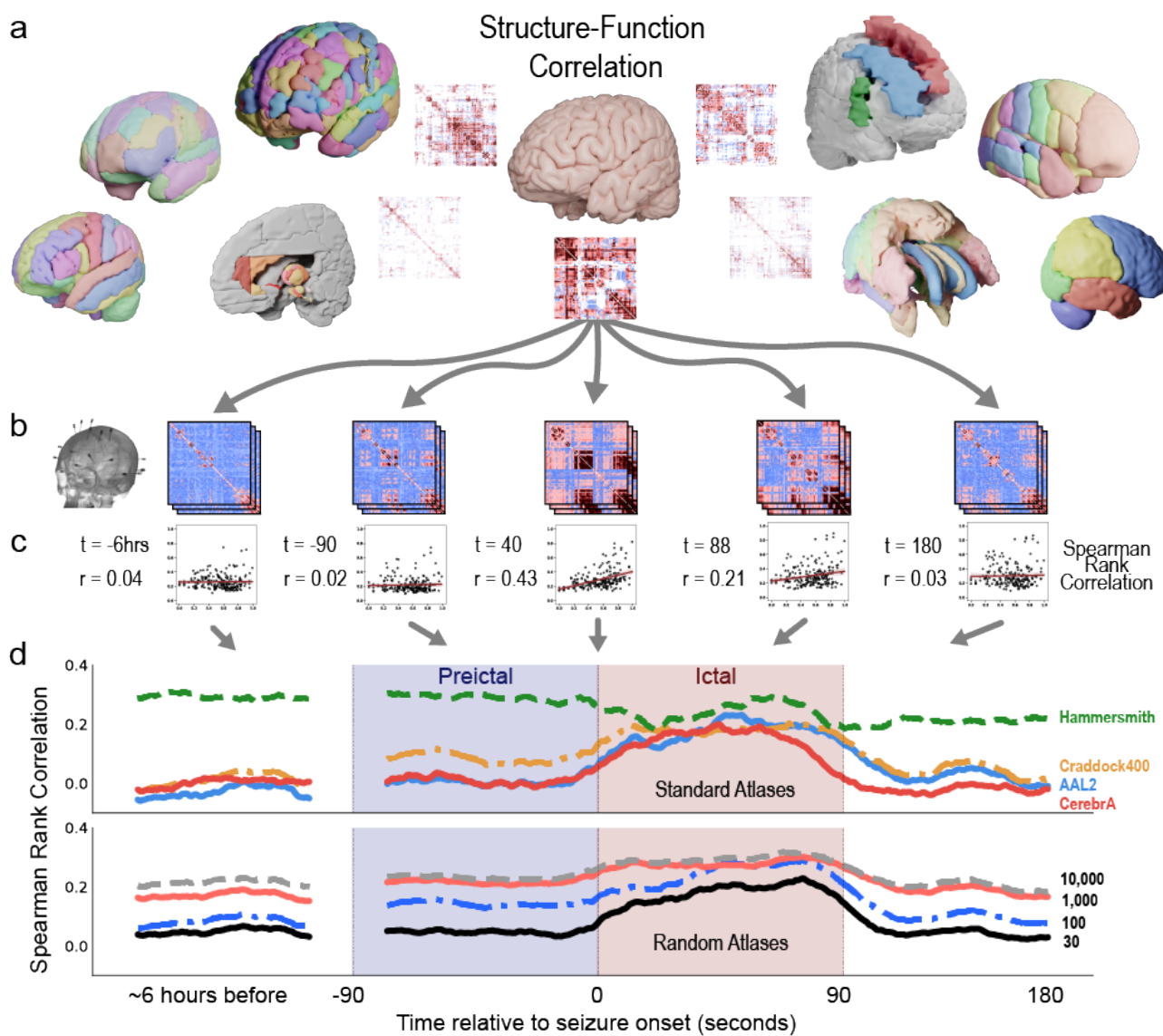


Fig. 4. Structure-Function correlation in a single patient using different atlases. | **a**, Example atlases and structural connectivity matrices. **b**, Functional connectivity matrices are computed from SEEG recordings during the interictal, preictal, ictal, and postictal periods. During each period, the SEEG data is binned into non-overlapping windows (the vertically stacked matrices) to create time varying representations of functional connectivity. Broadband cross correlation matrices are shown for sub-patient07 at 6 hours before seizure onset, 90 seconds before seizure onset, 40 seconds after seizure onset ($t = 40$), 88 seconds after seizure onset (seizure duration = 89 seconds), and 180 seconds after seizure onset (or 91 seconds after seizure termination). **c**, Each functional connectivity matrix is correlated to a structural connectivity matrix of a given atlas. Spearman Rank Correlation is measured between all time points and all atlases for each patient. Lines of best fit are for visualization purposes only. **d**, SFC is graphed at each time point for four example standard atlases (Hammersmith, Craddock400, AAL2, and CerebrA), and four example random atlases (30, 100, 1k, and 10k parcellations). SFC increases during seizure state for some standard atlases (Craddock 400, AAL2, and CerebrA atlases). This result follows previous SFC publications with ECoG^{13,14}. However, SFC does not increase for the Hammersmith atlas. These findings highlight that the power to detect a change in the structure-function correlation at seizure onset, and thus the ability to probe the hypothesis that seizure activity is correlated to brain structure, may be reduced using some atlases. The use of different atlases may contradict previous studies.

134 seizure onset ($t = -90$), 40 seconds after seizure onset ($t = 40$), 88 seconds after seizure onset (seizure duration = 89
 135 seconds), and 180 seconds after seizure onset (91 seconds after
 136 seizure termination). Each functional connectivity matrix
 137

138 time window was correlated to each structural connectivity
 139 matrix, yielding a SFC at each time window (Fig. 4c). Each
 140 point represents the structural edge weight between two brain
 141 regions and their corresponding functional connectivity edge

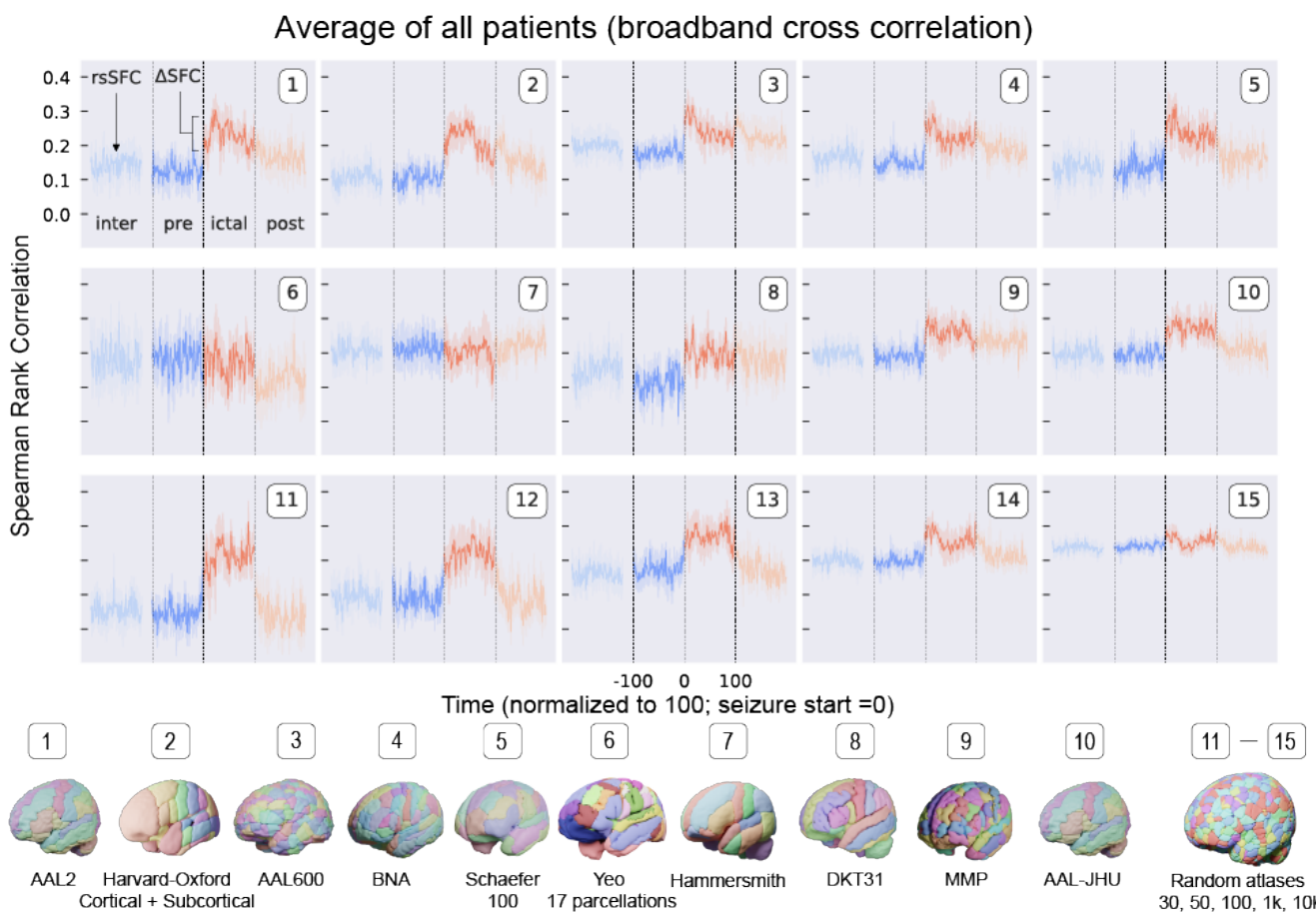


Fig. 5. Structure-Function Correlation in multiple patients using different atlases. | SFC for ten standard atlases and five random atlases using SEEG broadband cross-correlation matrices averaged across all patients with clinically annotated seizures ($N = 10$). Resting state SFC (rsSFC) is the SFC during the interictal period. The change from preictal to ictal SFC is Δ SFC. SFC was similarly calculated for random atlases and shows that rsSFC and Δ SFC may change with parcellation scale. These findings may be concerning given that the *inherent* structure-function relationship in the brain is not necessarily changing at resting state, but its measurement is greatly affected by atlas choice alone.

142 weight in broadband cross-correlation. A line of best fit is
 143 shown for visualization, and r values represent Spearman rank
 144 correlation for that time point. SFC was graphed for all
 145 time points during the interictal, preictal, ictal, and postictal
 146 periods for this patient in Fig. 4d.

147 Four example standard and random atlases are graphed.
 148 We show that SFC increases during the ictal state for many
 149 atlases (CerebrA, AAL2, Craddock 400), but not all atlases
 150 (Hammersmith). The increase in SFC during seizures follows
 151 previous SFC studies using ECoG ^{13,14}. Similarly, SFC in-
 152 creases for a subset of random whole-brain atlases. While
 153 parcellation scale may affect SFC, it is not the only feature
 154 affecting SFC – the Hammersmith and AAL2 atlases have
 155 similar parcellation scales yet diverging neuroanatomical prop-
 156 erties and SFC dynamics. These findings highlight inference
 157 from one type of atlas may suggest that seizure activity is not
 158 correlated to brain structure, contradicting previous studies ¹³.

159 **Varying atlases affect SFC: multiple subjects.** Fig. 5 shows
 160 SFC for ten standard atlases and five random atlases using

161 SEEG broadband cross-correlation metrics averaged across
 162 all patients with clinically annotated seizures ($N = 10$). The
 163 AAL2 atlas shows a statistically significant increase in SFC
 164 from preictal to ictal periods ($p < 0.05$ by Wilcoxon signed
 165 rank test after Bonferroni correction for 55 tests). This change
 166 from preictal to ictal SFC is denoted Δ SFC. Using the AAL2
 167 atlas, this finding supports the hypothesis that seizure activity
 168 propagates and spreads via axon tracts making up the underly-
 169 ing structural connectivity of the brain ^{13,14}. SFC was similarly
 170 calculated for random whole-brain atlases. A notable finding
 171 is that during the interictal period, resting state SFC (rsSFC)
 172 increases at larger number of parcellations (i.e. smaller parcel-
 173 lation volumes). We show that rsSFC is observably affected by
 174 parcellation scale when plotting the random atlases in Fig. 5
 175 (bottom row). These findings may be concerning given that
 176 the *inherent* structure-function relationship in the brain is not
 177 necessarily changing at resting state, but its measurement is
 178 greatly affected by atlas choice alone.

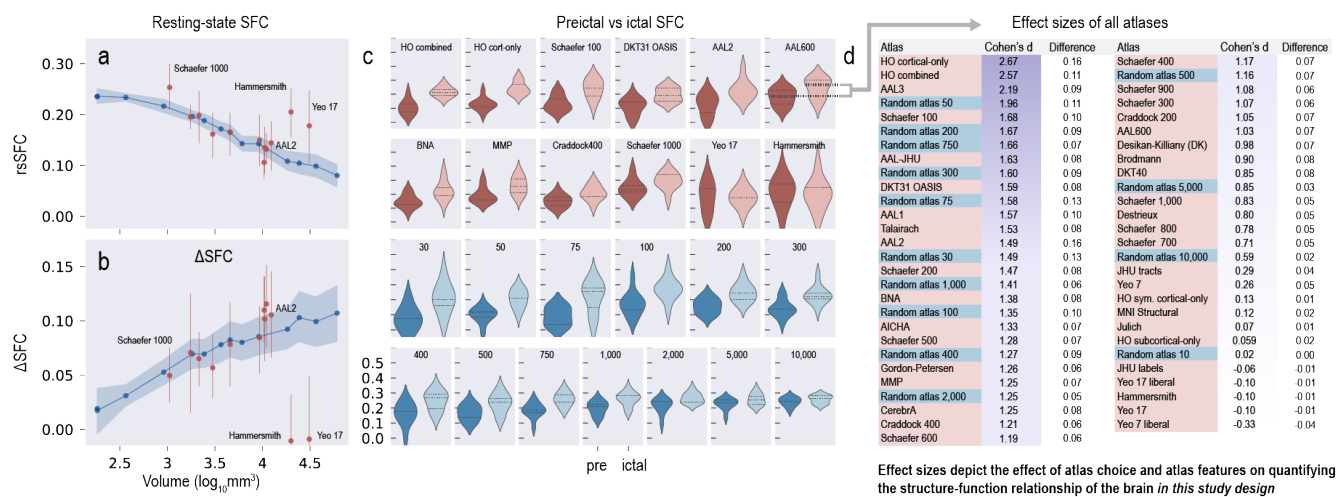


Fig. 6. The power to test a hypothesis about epilepsy pathophysiology changes depending on atlas choice | a, Resting state SFC (rsSFC) decreases with larger parcellation volumes (moving left to right). Random atlases are shown in blue, and select standard atlases are shown in red. Points represent the average across all patients, and bands represent 95% confidence intervals. b, Δ SFC increases with larger parcellation volume (moving left to right). Broadly, $|\Delta$ SFC may be interpreted as the change in SFC with respect to disease (e.g. a seizure) and non-disease states, and this change has been used to characterize and make inferences on many neurological diseases. These results exemplify that parcellations that are either too coarse (large volumes) or too fine (small volumes) may not adequately capture the underlying SFC of the brain or its dynamics with relation to a neurological disease. c, A subset of atlases show a difference in preictal and ictal SFC. d, The effect size between preictal and ictal SFC is calculated for all 55 atlases used in this study. Many atlases commonly used in the neuroscience literature have comparable effect sizes to random atlases. The standard atlases with the greatest effect size (and thus power) are the Harvard-Oxford and AAL3 atlases. These atlases outperform many random atlases (where anatomical boundaries are not followed) and may indicate that their parcellation scheme captures the structure-function relationship in the brain at seizure onset with DTI and iEEG.

179 **Varying atlases affect resting state SFC and Δ SFC.** Resting state SFC (rsSFC) and the change in SFC (Δ SFC) from 180 preictal to ictal periods are affected by parcellation scale 181 (Fig. 6). Fig. 6a shows how rsSFC *decreases* with larger average 182 parcellation volumes (moving left to right). A large average 183 parcellation volume for a given atlas generally means there is 184 a fewer number of total parcellations (e.g. the MNI structural 185 atlas has a large average parcellation volume given only nine 186 parcellations). In contrast, Fig. 6b shows Δ SFC *increases* with 187 larger parcellation volumes (moving left to right). Broadly, 188 Δ SFC may be interpreted as the change in SFC with respect to 189 a disease (e.g. a seizure) and non-disease states. This change 190 metric has been used to characterize and make inferences in 191 many neurological disorders^{31,32}. Only a subset of atlases 192 show a change in SFC at seizure onset (Fig. 6c). These results 193 exemplify that either overly coarse or fine parcellations may 194 not adequately capture the underlying SFC of the brain or its 195 dynamics with relation to a neurological disease.

196 **Atlas choice affects the power to test a hypothesis.** The effect 197 size between preictal and ictal SFC is calculated for all 55 198 atlases used in this study (Fig. 6d). Cohen's d and the 199 difference between the mean ictal and mean preictal SFC are 200 shown. Atlases are ordered by Cohen's d.

201 We found that different atlases may alter the power to test 202 the hypothesis about epilepsy pathophysiology that seizures 203 propagate through the underlying structural tracts of the 204 brain, measured with diffusion MRI. This hypothesis has been 205

previously supported in prior studies^{13,14,23,24}

206 Many atlases commonly used in the neuroscience literature 207 have comparable effect sizes to random atlases (where anatomical 208 boundaries are not followed). The standard atlases with 209 the greatest effect size (and thus power, given equal significance 210 levels and sample sizes) are the Harvard-Oxford and 211 AAL3 atlases. These atlases outperform many random atlases 212 and may indicate that their parcellations may adequately capture 213 the structure-function relationship in the brain. These 214 atlases may capture the "true" structural network architecture 215 (see Fig. 1c) because these network architectures better differentiate 216 and are more correlated to functional changes seen at 217 seizure onset.

218 Despite the effect sizes of the Harvard-Oxford and AAL3 219 atlases, however, there may not be a "true gold standard" atlas 220 or parcellation scheme given that resolution is more critical 221 than the exact border location of parcels²⁹, there may be 222 no single functional atlas for an individual across all brain 223 states²⁸, and many standard atlases yield similar effect sizes 224 to randomly generated atlases (this study).

225 Discussion

226 In this study, we performed an extensive evaluation of the 227 available structural, functional, random, and multi-modal 228 atlases in the neuroscience literature (Table 1). We detailed 229 morphological (Fig. 2) and network (Fig. 3) differences 230 between these atlases. We showed the effect of atlas choice on 231



Fig. 7. A Framework for brain atlases. | **a**, Which atlas should be chosen for a study? We propose a framework that helps select an atlas in the context of its descriptive, explanatory, and predictive validity. **Descriptive validity** means the features of an atlas appropriately resembles the experimental system. An atlas is also a *tool* to solve a variety of problems in neuroscience. It may be used as part of a *methodology* to explain causality (**explanatory validity**), or it may be used to make predictions (**predictive validity**). These two goals are distinct, and the differences between explanation and prediction "must be understood for progressing scientific knowledge" ¹⁵. These aspects (to explain or to predict) should be considered when selecting an atlas. **b**, Non-mutually exclusive atlas features related to descriptive validity. **c**, A list of questions to consider when choosing an atlas. Gray lines connect related questions. **d**, An algorithm for atlases selection *a priori* and *post hoc*. Please see the main text for further details.

232 the measurement of structure-function correlation (SFC) in
233 epilepsy patients (Fig. 4 and Fig. 5). We also showed how
234 various atlases may affect the power to test a hypothesis about
235 seizure propagation (Fig. 6). This work has implications for
236 investigators because the ability to test hypotheses and make
237 predictions about the brain's function may depend on atlas
238 choice. In light of our study using an extensive list of available
239 brain atlases, we propose a general framework below for
240 evaluating and selecting an atlas (Fig. 7).

241 **A Framework for Brain Atlases.** Various publications have
242 highlighted the Atlas Concordance Problem^{2-4,9}, curated several
243 atlases in freely accessible databases^{33,34}, and made arguments
244 for why specific atlas features (Fig. 7b) may be superior
245 in certain situations^{21,28,35-39}. There have been great efforts
246 to publish accurate and precise parcellations as seen with
247 an exponential rise in atlas-related publications over the last
248 three decades (Fig. S8). However, none have found a general
249 solution to the underlying problem: Does atlas choice matter?

250 We provide a framework that allows us to determine if
251 the choice of an atlas is appropriate in the context of its (1)
252 descriptive, (2) explanatory, and (3) predictive validity²⁶. This
253 framework is borrowed from the logic for assessing network
254 models²⁶, animal models,^{25,40}, and psychometric tests^{27,41},
255 where assessment of these models with standard statistical
256 model-selection methods is particularly challenging. Thus,
257 theoretical constructs already formulated in other fields may
258 provide guidance.

259 **Descriptive validity** of an atlas refers to an atlas that
260 appropriately resembles the system in which we work. In other
261 words, it has "face value"²⁵. An atlas should include features
262 (Fig. 7b) relevant to the study (e.g., parcellations containing
263 subcortical structures relevant to epilepsy). Importantly, the
264 descriptive validity of an atlas also relates to the modality scale
265 we use to measure the brain – for example, DWI and fMRI
266 at the macroscale⁴², iEEG and tracers at the meso scale⁴³,
267 and microscopy at the microscale⁴⁴. It is important to select
268 a parcellation scale that resembles the measurement modality
269 resolution (Fig. 6a). When correlating DWI with iEEG in
270 our study at larger parcellation sizes, we lose our ability to
271 discern precise anatomical locations that are structurally and
272 functionally related (Fig. 6b). Similarly at smaller parcellation
273 sizes (tending to voxel resolution), we may not capture the "true"
274 structural network architecture (Fig. 1c), and thus we lose our
275 ability to capture structure-function relationship changes at seizure
276 onset.

277 An atlas is a *tool* to tackle a wide variety of problems in
278 neuroscience. It may be part of a methodology to explain causality
279 (**explanatory validity**) or it may be part of a methodology to
280 make predictions (**predictive validity**). These two goals are
281 distinct, and the differences between explanation and prediction
282 "must be understood for progressing scientific knowledge"
283 as described in "To Explain or Predict?" by Shmueli, 2010¹⁵.
284 In the context of building scientific models, a model with a
285 high explanatory ability may not have a high predictive ability.

286 Similar to models, atlases are also part of a scientific *methodology*
287 to (1) explain how the brain functions or (2) predict new
288 observations (i.e., they are one part of the overall method-
289 ological pipeline to test hypotheses or make predictions about
290 the brain - for studies using atlases). Thus, atlases are tools.
291 An atlas may be suitable for hypothesis testing, for example,

292 because it includes subcortical structures like the hippocampus
293 (also high descriptive validity) to support a hypothesis about
294 seizure propagation through subcortical structures. Intuitively,
295 without subcortical structures, it would be impossible to test
296 hypotheses about subcortical structures. Less intuitively, ex-
297 planatory validity of an atlas may also relate to the *power* to
298 test hypotheses, which we show in our study. Some atlases
299 may not be suitable for scientific inquiry because they provide
300 little statistical power to detect differences in disease states, for
301 example, to detect changes in SFC at seizure onset (Fig. 6b).
302 It may be impossible to accurately predict power using an
303 atlas before conducting a study, however, other studies asking
304 similar questions using similar atlases may provide reasonable
305 estimates of effect sizes (our study has similar effect sizes to a
306 previous study¹³). Power may also depend on the accuracy of
307 anatomical boundaries, or in our study, other atlas features
308 such as parcellation scale and configuration (Fig. 6d). For
309 example, the Harvard-Oxford and AAL3 atlases have similar
310 parcellation configurations and similar power.

311 Some atlases may or may not be suitable for making
312 predictions about new or future observations about the
313 brain. For example, many network properties change with
314 atlas choice (Fig. 3), and thus it is reasonable to suspect model
315 prediction outputs may change with respect to the atlas used
316 to build and train such models. Importantly, the exclusion
317 of some anatomical structures, like white matter or the cere-
318 bellum in some atlases, may affect the training data used to
319 build predictive models. In our study, a translational goal
320 is to predict functional seizure activity from structural data.
321 SEEG records activity from both gray matter and white matter;
322 however, recent studies have shown that white matter
323 functional recordings may provide different information than
324 gray matter⁴⁵⁻⁴⁸. Thus, excluding some anatomical labels may
325 affect model predictions. Another example is the use of net-
326 work models to predict spread, such as α -synuclein across the
327 brain connectome⁴⁹. Without the incorporation of all brain
328 structures related to α -synuclein spread, models to predict
329 and monitor spread may be inaccurate.

330 **Are accurate anatomical or functional parcellations needed?**
331 During the course of conducting this study, and while undergo-
332 ing peer review, other atlases with more accurate or relevant
333 parcellations to the study's population were published in dif-
334 ferent areas of neuroscience⁵⁰⁻⁵⁸. Here, we cautiously propose
335 a question: Are efforts to publish more atlases created with
336 different algorithms or slightly modified parcellations from
337 existing atlases providing any advantages over already existing
338 atlases? Naturally, accurate and precise parcellations are
339 needed when probing specific hypotheses about exact struc-
340 tures that depend on accurate segmentation of such structures
341 (particularly at the sub-field or cellular level); however, few
342 studies compare an atlas to a null atlas (one with randomly
343 generated parcellations). Studies that do are Gordon et al.
344 2016⁵⁹ and Lewis et al. 2021⁵⁸.

345 In this study, we show that random atlases provide similar
346 power to detect differences in SFC between preictal and ictal
347 states (Fig. 6d). Indeed, it is difficult or nearly impossible to
348 evaluate a newly proposed atlas, given that the performance
349 metrics to evaluate an atlas may be infinite (given infinite
350 experimental designs). Only one such metric, SFC, was used
351 in this study. But given new deep learning methods and other

352 computationally expensive methods using trained classifiers for
353 segmentation, existing atlases may be adequate for labs with
354 limited funding resources, trained personnel, and access to
355 GPUs. These labs may still be capable of answering important
356 questions in neuroscience.

357 **Which atlas should be used for my study?** One of the most
358 difficult challenges as scientific investigators is to make optimal
359 methodological decisions to discover useful findings for the
360 scientific community. Selecting an atlas is one such decision we
361 may make in some of our studies. We realize the framework
362 provided above may be abstract to some readers; we also
363 provide a concrete list of questions to consider when choosing
364 an atlas (Fig. 7c) for a neuroimaging study. However, in
365 conducting this study, we also found that researchers may face
366 three problems when choosing an atlas (Fig. 7d) and these
367 problems are worth further discussion. The first two problems
368 are in selecting an atlas *a priori*, or before conducting a study.
369 They deal with selecting one or a few atlases to preserve power,
370 or in selecting a standard set of atlas to publish public data
371 for other researchers to use. The third problem is the issue of
372 conflicting results between two atlases and what to do after a
373 study is conducted (*post hoc*). We provide a further discussion
374 on these problems below.

375 **Considerations in selecting one or a few atlases.** Selecting
376 one atlas may preserve power and avoid a multiple comparisons
377 problem by testing every atlas. Selecting an additional atlas
378 may also be chosen to confirm the robustness of results. In
379 these cases, a balance of time, availability of tools, and atlas
380 features logical for your study as outlined in Fig. 7a-c need to
381 be considered. For example, if a custom atlas is used, how will
382 that affect replicability and meta analysis in the long-run for
383 the field? What are the atlas features needed (such as scale
384 and coverage of regions)? What are the computational costs
385 and personnel training needed to use particular atlases? (See
386 questions in Fig. 7c).

387 **Considerations in selecting a standard set of atlases.** When
388 publishing results and/or making data publicly available for
389 other investigators to use, another approach is to select a set
390 of atlases based on the perceived needs of other investigators,
391 atlas features covered, prevalence of atlases used in the literature
392 (Fig. S9a), and the prevalence of "turn-key" neuroimaging
393 software that incorporate these atlases (Fig. S9b). Studies are
394 emerging with data publicly available for use based on one or a
395 few select atlases^{60,61}. Many turn-key neuroimaging software
396 also inevitably have to make the decision to employ a set of
397 atlases to meet the needs of many researchers. A problem may
398 arise, however, when other researchers need the published data
399 at other atlas resolutions or with other structures. And unfor-
400 tunately, the value of the data may be lessened and the effort
401 put in by the publishing researchers may be in waste if this
402 happens. What may help with the atlas concordance problem
403 is perhaps a "standard set" of atlases – a set to benchmark
404 studies across the neuroimaging field. Furthermore, turn-key
405 tools like FreeSurfer, QSIprep, DSI-studio, FSL, and many
406 others may benefit from a standard set of incorporated atlases
407 that captures enough features useful to the majority of the
408 neuroscience community, even if not every available atlas is
409 included. Based on our exhaustive search of atlases in the

410 neuroimaging literature, the ability to collect them for use
411 in a single study, the prevalence of certain atlases already
412 in-use (Fig. S9a), and the prevalence of neuroimaging software
413 (Fig. S9b) we propose an initial set of atlases (Fig. 7d).

414 The AAL atlas is one of the most commonly used vol-
415 umetric atlases (Fig. S9a), and along with the Harvard-Oxford
416 atlas, may provide complimentary results when published
417 together. The Brainnetome atlas⁶² is another structural at-
418 lases at a finer resolution, having gained popularity since its
419 introduction in 2016. The Destrieux and DKT atlases are
420 also structural atlases, and already incorporated into one of
421 the most commonly used neuroimaging software, FreeSurfer
422 (<https://surfer.nmr.mgh.harvard.edu>). FreeSurfer provides
423 surface-based registration, which may more accurately label
424 cortical structures than volumetric registration (Fig. S6). Accu-
425 rate segmentation of sub-cortical structures may also be
426 acquired from FSL⁶³ (<https://fsl.fmrib.ox.ac.uk/fsl/fslwiki>). In
427 addition, the MMP, or "Glasser" atlas was created from
428 multi-modal imaging data. A commonly used atlas provided
429 at different scales is Schaefer atlases provide, however, it does
430 not include subcortical structures.

431 Random atlases may also provide robust conclusions by
432 allowing researchers to manipulate the resolution, size, and
433 shape of parcellations and iterate over many atlases. Although
434 random parcellations may forgo accuracy because they do
435 not follow true anatomical boundaries, these atlases may still
436 provide similar conclusions to other standard atlases with the
437 added benefit of permuting results over many atlases (Fig. 6).
438 An alternative to random atlases is to divide or combine the
439 parcellations of another standard atlas (a "derived" atlas in
440 Fig. 7d). For example, the AAL 600 is derived from the AAL
441 atlas in which its parcellations are further sub-divided using
442 a specified algorithm. Parcellations may also be sub-divided
443 randomly.

444 **Considerations in conflicting results between atlases.** When
445 more than one atlas is used, results may conflict. We define
446 conflicting results as two different atlases giving alternating
447 predictions (e.g., good vs poor outcomes, increase in SFC
448 rather than decrease in SFC) or support alternating working
449 hypotheses (e.g., the temporal lobe is involved in one atlas,
450 but another atlas highlights the involvement of the frontal
451 lobe in the pathophysiology of a disease). We do not mean
452 that conflicting results arise due to lack of statistical power
453 (e.g., one atlas gives a p-value of 0.06 and another atlas 0.04).

454 One way to understand if the observed effect is not an
455 artifact of the atlas choice is to select a few atlases with
456 varying features and figure out what is causing the conflict.
457 Unfortunately, there may be no other way given that every
458 study will have different parameters and measurements to know
459 what gives rise to conflicting results. In the matter where
460 conflicting results arise due to atlas selection, then it may
461 troubleshooting may be needed to understand what gives rise
462 to the conflict (surface vs volumetric registration, parcellation
463 scale, missing relevant structures, etc.). Fortunately, however,
464 most atlases in this study affect power rather than conflicting
465 results (Fig. 6d). We hope this discussion, our study, and our
466 figures provide insight to others.

467 **Limitations.** Our study is not without limitations. A major
468 limitation is that we did not evaluate atlases in a diverse set

469 of experimental systems, but rather limited our analysis to a
470 contemporary topic in epilepsy using SEEG implantations and
471 to a study of the structure-function of the brain, potentially
472 appealing to a wider audience. The question we were trying to
473 answer ("Which atlas should we use?") is a difficult problem to
474 solve, given that it would be impossible to evaluate all atlases
475 in all experimental designs. We attempted to generalize a
476 framework given our findings after an extensive search for, and
477 curation of, available neuroimaging atlases.

478 We also did not perform a feature selection analysis post-
479 hoc to maximize ΔSFC at seizure onset; rather, we performed
480 a comprehensive evaluation of many atlases to set a general
481 framework and describe the nuances between the different
482 atlases and their features. Ideally in our study, we required
483 a whole-brain, volumetric atlas that covered the implanted
484 SEEG electrode contacts. No such atlas existed. We opted for
485 combining different atlases or developing randomly parcellated
486 atlases used in previous publications^{30,64}. However, no general
487 framework existed to determine which atlas should be used
488 or clearly outlined the feature space of these atlases. We had
489 no formal basis for how changing an atlas could change our
490 results and eventual goal for translating network models to
491 better treat epilepsy patients.

492 Another limitation, we assume a change in SFC supports
493 the hypothesis that seizures harness the underlying structural
494 connectome of the brain (along with support from prior literature^{13,14,65}). We may be biasing our results to select an
495 atlas that maximizes ΔSFC . However, we wish to select a
496 methodology that allows us to measure *any change* in brain
497 state that accompanies seizure onset (explanatory validity),
498 permitting us to probe epilepsy biology and understand the
499 processes that govern seizure spread.

500 An additional limitation concerns the effect of parcellation
501 volume on SFC. In probing this effect across our random
502 atlases and atlases used in the literature, we did not perform
503 controlled experiments to separate the effects of parcellation
504 size from parcellation N (number of parcellations). A future
505 experiment could fix the number of parcellations while changing
506 parcellation volume (or vice versa). This would allow us
507 to test whether parcellation volume or N drives changes in
508 SFC. However, this was outside the scope of our study.

509 Our goal was to highlight the importance of selecting an
510 appropriate atlas from an array of possibilities, using a data-
511 driven, validated experimental paradigm¹³. We acknowledge
512 new studies that show that streamline counts may not com-
513 pletely reflect the underlying diffusion data⁶⁶; however, com-
514 paring such techniques were outside the scope and goal of our
515 focused study. We also note that few patients had lesions
516 on imaging. Misalignment due to non-linear distortion may
517 add noise to our data; however, few patients had lesions. Our
518 study was not conducted to necessarily make the claim that
519 SFC changes exist in the brain at seizure onset, but rather to
520 show how varying atlases may change SFC.

521 Finally, our analysis relies on the assumption that an atlas
522 approach must be used to quantify SFC and does not consider
523 an atlas-agnostic approach nor if such an approach is appro-
524 priate. To study SFC using networks, both structural and
525 functional networks must have nodes representing the same
526 entity – neuroanatomical structures. The atlases defining
527 anatomical structures (whether they are functionally, histolog-

528 ically, genetically, procedurally, multi-modally, or randomly
529 defined) are the link between structural connectivity and func-
530 tional connectivity measurements of the brain. To study SFC,
531 we must rely on the neuroanatomical structures defined by
532 an atlas, then localize electrodes to these regions and corre-
533 late the structural measurements (e.g., streamlines, fractional
534 anisotropy, mean diffusivity) with functional measurements
535 (e.g., cross-correlation, coherence, mutual information). Fun-
536 damentally, we are defining the nodes of the brain in advance,
537 which can alter our results; a more comprehensive discussion
538 on defining the nodes of the brain are in Fornito et al., 2016
539 and Bijsterbosch et al., 2017^{43,67}.

540
541 **Conclusion.** The publication of atlases and their distribution
542 across neuroimaging software platforms has risen exponentially
543 over the last three decades. Our study illustrates the
544 critical need to evaluate the reproducibility of neuroscience
545 research using atlases published alongside tools and analysis
546 pipelines already established in the neuroscience community
547 (e.g., FreeSurfer, DSI studio, FSL, SPM, QSIprep, fMRIprep,
548 MRIcron, ANTs, and others).

References

- [1] Klein, A. & Tourville, J. 101 Labeled Brain Images and a Consistent Human Cortical Labeling Protocol. *Frontiers in Neuroscience* **6** (2012).
- [2] Mandal, P. K., Mahajan, R. & Dinov, I. D. Structural brain atlases: design, rationale, and applications in normal and pathological cohorts. *Journal of Alzheimer's disease : JAD Suppl 3*, S169–88 (2012).
- [3] Dickie, D. A. et al. Whole Brain Magnetic Resonance Image Atlases: A Systematic Review of Existing Atlases and Caveats for Use in Population Imaging. *Front Neuroinform* **11**, 1 (2017).
- [4] Bohland, J. W., Bokil, H., Allen, C. B. & Mitra, P. P. The Brain Atlas Concordance Problem: Quantitative Comparison of Anatomical Parcellations. *PLoS ONE* **4**, e7200 (2009).
- [5] Beal, D. S. et al. The trajectory of gray matter development in Broca's area is abnormal in people who stutter. *Frontiers in Human Neuroscience* **9** (2015).
- [6] Van Horn, J. D. et al. Mapping Connectivity Damage in the Case of Phineas Gage. *PLoS ONE* **7**, e37454 (2012).
- [7] Barker, F. G. Phineas among the phrenologists: the American crowbar case and nineteenth-century theories of cerebral localization. *Journal of Neurosurgery* **82**, 672–682 (1995).
- [8] Mazzuotta, J. et al. A probabilistic atlas and reference system for the human brain: International Consortium for Brain Mapping (ICBM). *Philosophical Transactions of the Royal Society of London. Series B: Biological Sciences* **356**, 1293–1322 (2001).
- [9] Evans, A. C., Janke, A. L., Collins, D. L. & Baillet, S. Brain templates and atlases. *NeuroImage* **62**, 911–22 (2012).
- [10] National Geographic Society Encyclopedic entry. *Atlas* (2022). URL <https://www.nationalgeographic.org/encyclopedia/atlas/>.
- [11] National Geographic Society Encyclopedic entry. *Border* (2022). URL <https://www.nationalgeographic.org/encyclopedia/border/>.
- [12] Van Essen, D. C. et al. The WU-Minn Human Connectome Project: an overview. *NeuroImage* **80**, 62–79 (2013).
- [13] Shah, P. et al. Characterizing the role of the structural connectome in seizure dynamics. *Brain: A Journal of Neurology* (2019).
- [14] Ashourvan, A. et al. Pairwise maximum entropy model explains the role of white matter structure in shaping emergent co-activation states. *Commun Biol* **4** (2021).
- [15] Shmueli, G. To Explain or to Predict. *Statistical Science* **25** (2010).
- [16] Makris, N. et al. Decreased volume of left and total anterior insular lobule in schizophrenia. *Schizophrenia Research* **83**, 155–171 (2006).
- [17] Hammers, A. et al. Three-dimensional maximum probability atlas of the human brain, with particular reference to the temporal lobe. *Human Brain Mapping* **19**, 224–247 (2003).
- [18] Thomas Yeo, B. T. et al. The organization of the human cerebral cortex estimated by intrinsic functional connectivity. *J Neurophysiol* **106**, 1125–65 (2011).
- [19] Schaefer, A. et al. Local-Global Parcellation of the Human Cerebral Cortex from Intrinsic Functional Connectivity MRI. *Cerebral Cortex* **28**, 3095–3114 (2018).
- [20] Glasser, M. F. et al. A multi-modal parcellation of human cerebral cortex. *Nature* **536**, 171–178 (2016).
- [21] Coalson, T. S., Van Essen, D. C. & Glasser, M. F. The impact of traditional neuroimaging methods on the spatial localization of cortical areas. *Proceedings of the National Academy of Sciences* **115**, E6356–E6365 (2018).
- [22] Wu, Z., Xu, D., Potter, T., Zhang, Y. & The, A. D. N. I. Effects of Brain Parcellation on the Characterization of Topological Deterioration in Alzheimer's Disease. *Frontiers in Aging Neuroscience* **11**, 113 (2019).
- [23] Proix, T., Bartolomei, F., Guye, M. & Jirsa, V. K. Individual brain structure and modelling predict seizure propagation. *Brain : a journal of neurology* **140**, 641–654 (2017).

600 [24] Wirsich, J. *et al.* Whole-brain analytic measures of network communication reveal increased
601 structure-function correlation in right temporal lobe epilepsy. *NeuroImage. Clinical* **11**, 707–
602 718 (2016).

603 [25] Willner, P. The validity of animal models of depression. *Psychopharmacology* **83**, 1–16
604 (1984).

605 [26] Bassett, D. S., Zurn, P. & Gold, J. I. On the nature and use of models in network neuroscience.
606 *Nature Reviews Neuroscience* **19**, 566–578 (2018).

607 [27] Association, A. P. Technical recommendations for psychological tests and diagnostic tech-
608 niques. *Psychological bulletin* **51**, 1–38 (1954).

609 [28] Salehi, M. *et al.* There is no single functional atlas even for a single individual: Functional
610 parcel definitions change with task. *NeuroImage* **208**, 116366 (2020).

611 [29] Albers, K. J. *et al.* Using connectomics for predictive assessment of brain parcellations. *Neu-
612 roImage* **238**, 118170 (2021).

613 [30] Zalesky, A. *et al.* Whole-brain anatomical networks: does the choice of nodes matter? *Neu-
614 roImage* **50**, 970–983 (2010).

615 [31] Cocchi, L. *et al.* Disruption of structure-function coupling in the schizophrenia connectome.
616 *NeuroImage. Clinical* **4**, 779–874 (2014).

617 [32] Sathian, K. & Crosson, B. Structure-function correlations in stroke. *Neuron* **85**, 887–9 (2015).

618 [33] Gorgolewski, K. J. *et al.* NeuroVault.org: a web-based repository for collecting and sharing
619 unthresholded statistical maps of the human brain. *Frontiers in neuroinformatics* **9**, 8 (2015).

620 [34] Lawrence, R. M. *et al.* Standardizing human brain parcellations. *Scientific data* **8**, 78 (2021).

621 [35] Alexander, B. *et al.* A new neonatal cortical and subcortical brain atlas: the Melbourne
622 Children's Regional Infant Brain (M-CRIB) atlas. *NeuroImage* **147**, 841–851 (2017).

623 [36] Brennan, B. P. *et al.* Use of an Individual-Level Approach to Identify Cortical Connectivity
624 Biomarkers in Obsessive-Compulsive Disorder. *Biological psychiatry. Cognitive neuroscience
625 and neuroimaging* **4**, 27–38 (2019).

626 [37] Cabezas, M., Oliver, A., Lladó, X., Freixenet, J. & Cuadra, M. B. A review of atlas-based
627 segmentation for magnetic resonance brain images. *Computer methods and programs in
628 biomedicine* **104**, e158–77 (2011).

629 [38] Caspers, S., Eickhoff, S. B., Zilles, K. & Amunts, K. Microstructural grey matter parcellation
630 and its relevance for connectome analyses. *NeuroImage* **80**, 18–26 (2013).

631 [39] Diedrichsen, J., Balsters, J. H., Flavell, J., Cussans, E. & Ramnani, N. A probabilistic MR
632 atlas of the human cerebellum. *NeuroImage* **46**, 39–46 (2009).

633 [40] Belzung, C. & Lemoine, M. Criteria of validity for animal models of psychiatric disorders:
634 focus on anxiety disorders and depression. *Biology of mood & anxiety disorders* **1**, 9 (2011).

635 [41] Association, A. E. R. (ed.) *Standards for Educational and Psychological Testing* (American
636 Educational Research Association, Lanham, MD, 2014).

637 [42] Sporns, O., Tononi, G. & Kötter, R. The human connectome: A structural description of the
638 human brain. *PLoS computational biology* **1**, e42 (2005).

639 [43] Fornito, A., Zalesky, A. & Bullmore, E. *Fundamentals of Brain Network Analysis* (Academic
640 Press, 2016).

641 [44] Sporns, O. The human connectome: a complex network. *Annals of the New York Academy
642 of Sciences* **1224**, 109–125 (2011).

643 [45] Greene, P., Li, A., González-Martínez, J. & Sarma, S. V. Classification of Stereo-EEG Con-
644 tacts in White Matter vs. Gray Matter Using Recorded Activity. *Frontiers in Neurology* **11**
645 (2021).

646 [46] Mercier, M. R. *et al.* Evaluation of cortical local field potential diffusion in stereotactic electro-
647 encephalography recordings: A glimpse on white matter signal. *NeuroImage* **147**, 219–232
648 (2017).

649 [47] Young, J. J. *et al.* Quantitative Signal Characteristics of Electrocorticography and Stereo-
650 electroencephalography: The Effect of Contact Depth. *Journal of clinical neurophysiology :
651 official publication of the American Electroencephalographic Society* **36**, 195–203 (2019).

652 [48] Revell, A. Y. *et al.* White Matter Signals Reflect Information Transmission Between Brain
653 Regions During Seizures. *bioRxiv* (2021).

654 [49] Henderson, M. X. *et al.* Spread of α -synuclein pathology through the brain connectome is
655 modulated by selective vulnerability and predicted by network analysis. *Nat Neurosci* **22**,
656 1248–1257 (2019).

657 [50] Wang, H. E. *et al.* VEP atlas: An anatomic and functional human brain atlas dedicated to
658 epilepsy patients. *J Neurosci Methods* **348**, 108983 (2021).

659 [51] Doucet, G. E. *et al.* Atlas55+: Brain Functional Atlas of Resting-State Networks for Late
660 Adulthood. *Cereb Cortex* **31**, 1719–1731 (2021).

661 [52] Munoz-Castañeda, R. *et al.* Cellular anatomy of the mouse primary motor cortex. *Nature*
662 **598**, 159–166 (2021).

663 [53] Huang, C.-C., Rolls, E. T., Feng, J. & Lin, C.-P. An extended Human Connectome Project
664 multimodal parcellation atlas of the human cortex and subcortical areas. *Brain Structure and
665 Function* (2021).

666 [54] Syversen, I. F. *et al.* Structural connectivity-based segmentation of the human entorhinal
667 cortex. *NeuroImage* **245**, 118723 (2021).

668 [55] Zhu, J. *et al.* Integrated structural and functional atlases of Asian children from infancy to
669 childhood. *NeuroImage* **245**, 118716 (2021).

670 [56] Joglekar, A. *et al.* A spatially resolved brain-region- and cell type-specific isoform atlas of the
671 postnatal mouse brain. *Nat Commun* **12**, 463 (2021).

672 [57] Callaway, E. M. *et al.* A multimodal cell census and atlas of the mammalian primary motor
673 cortex. *Nature* **598**, 86–102 (2021).

674 [58] Lewis, J. D., Bezgin, G., Fonov, V. S., Collins, D. L. & Evans, A. C. A sub+cortical fMRI-based
675 surface parcellation. *Human Brain Mapping* (2021).

676 [59] Gordon, E. M. *et al.* Generation and Evaluation of a Cortical Area Parcellation from Resting-
677 State Correlations. *Cerebral Cortex Cereb. Cortex* **26**, 288–303 (2016).

678 [60] Sinha, N. *et al.* Focal to bilateral tonic-clonic seizures are associated with widespread
679 network abnormality in temporal lobe epilepsy. *Epilepsia* **62**, 729–741 (2021). URL <https://onlinelibrary.wiley.com/doi/10.1111/epi.16819>.

680 [61] Royer, J. *et al.* An Open MRI Dataset for Multiscale Neuroscience. preprint, Neuroscience
681 (2021). URL <http://biorxiv.org/lookup/doi/10.1101/2021.08.04.454795>.

682 [62] Fan, L. *et al.* The Human Brainnetome Atlas: A New Brain Atlas Based on Connectional
683 Architecture. *Cerebral cortex (New York, N.Y. : 1991)* **26**, 3508–26 (2016).

684 [63] Perlaki, G. *et al.* Comparison of accuracy between FSL's FIRST and Freesurfer for caudate
685 nucleus and putamen segmentation. *Scientific Reports* **7**, 2418 (2017). URL <http://www.nature.com/articles/s41598-017-02584-5>.

686 [64] Mišić, B. *et al.* Cooperative and Competitive Spreading Dynamics on the Human Connectome.
687 *Neuron* **86**, 1518–29 (2015).

688 [65] Betzel, R. F. *et al.* Structural, geometric and genetic factors predict interregional brain con-
689 nectivity patterns probed by electrocorticography. *Nature Biomedical Engineering* (2019).

690 [66] Smith, R. E., Tournier, J. D., Calamante, F. & Connolly, A. SIFT2: Enabling dense quantitative
691 assessment of brain white matter connectivity using streamlines tractography. *NeuroImage*
692 **119**, 338–51 (2015).

693 [67] Bijsterbosch, J., Smith, S. M. & Beckmann, C. F. *An Introduction to Resting State fMRI
694 Functional Connectivity* (Oxford University Press, 2017).

695 [68] Wagenaar, J. B., Brinkmann, B. H., Ives, Z., Worrell, G. A. & Litt, B. A multimodal platform for
696 cloud-based collaborative research (IEEE, 2013).

697 [69] Kini, L. G., Davis, K. A. & Wagenaar, J. B. Data integration: Combined imaging and electro-
698 physiology data in the cloud. *NeuroImage* **124**, 1175–1181 (2016).

699 [70] Cieslak, M. *et al.* QSIPrep: an integrative platform for preprocessing and reconstructing
700 diffusion MRI data. *Nat Methods* **18**, 775–778 (2021).

701 [71] Fang-Cheng, Y., Wedeen, V. J. & Tseng, W.-Y. I. Generalized q-Sampling Imaging. *IEEE
702 Transactions on Medical Imaging* **29**, 1626–1635 (2010).

703 [72] Otsu, N. A Threshold Selection Method from Gray-Level Histograms. *IEEE Transactions on
704 Systems, Man, and Cybernetics* **9**, 62–66 (1979).

705 [73] Bonilha, L., Gleichgerrcht, E., Nesland, T., Rorden, C. & Fridriksson, J. Gray Matter Axonal
706 Connectivity Maps. *Frontiers in Psychiatry* **6** (2015).

707 [74] Park, B., Eo, J. & Park, H.-J. Structural Brain Connectivity Constraints within-a-Day Variability
708 of Direct Functional Connectivity. *Frontiers in Human Neuroscience* **11**, 408 (2017).

709 [75] Taylor, P. N. *et al.* The impact of epilepsy surgery on the structural connectome and its relation
710 to outcome. *NeuroImage. Clinical* **18**, 202–214 (2018).

711 [76] Fonov, V. *et al.* Unbiased average age-appropriate atlases for pediatric studies. *NeuroImage*
712 **54**, 313–327 (2011).

713 [77] Jenkinson, M., Beckmann, C. F., Behrens, T. E. J., Woolrich, M. W. & Smith, S. M. FSL.
714 *NeuroImage* **62**, 782–790 (2012).

715 [78] Dale, A. M., Fischl, B. & Sereno, M. I. Cortical Surface-Based Analysis. *NeuroImage* **9**,
716 179–194 (1999). URL <https://linkinghub.elsevier.com/retrieve/pii/S1053811998903950>.

717 [79] Maslov, S. Specificity and Stability in Topology of Protein Networks. *Science* **296**, 910–913
718 (2002).

719 [80] Litt, B. *et al.* Epileptic Seizures May Begin Hours in Advance of Clinical Onset. *Neuron* **30**,
720 51–64 (2001).

721 [81] Azarion, A. A. *et al.* An open-source automated platform for three-dimensional visualization
722 of subdural electrodes using CT-MRI coregistration. *Epilepsia* **55**, 2028–2037 (2014).

723 [82] Ludwig, K. A. *et al.* Using a common average reference to improve cortical neuron recordings
724 from microelectrode arrays. *Journal of neurophysiology* **101**, 1679–89 (2009).

725 [83] Kramer, M. A. *et al.* Coalescence and fragmentation of cortical networks during focal seizures.
726 *The Journal of neuroscience : the official journal of the Society for Neuroscience* **30**, 10076–
727 85 (2010).

728 [84] Khambhati, A. N. *et al.* Dynamic Network Drivers of Seizure Generation, Propagation and Ter-
729 mination in Human Neocortical Epilepsy. *PLoS computational biology* **11**, e1004608 (2015).

730 [85] Khambhati, A. N., Davis, K. A., Lucas, T. H., Litt, B. & Bassett, D. S. Virtual Cortical Resection
731 Reveals Push-Pull Network Control Preceding Seizure Evolution. *Neuron* **91**, 1170–1182
732 (2016).

733 [86] Khambhati, A. N. *et al.* Recurring Functional Interactions Predict Network Architecture of
734 Interictal and Ictal States in Neocortical Epilepsy. *eNeuro* **4**, ENEURO.0091–16.2017 (2017).

735 [87] Newsom, J. J. & Thiagarajan, T. C. EEG Frequency Bands in Psychiatric Disorders: A Review
736 of Resting State Studies. *Frontiers in Human Neuroscience* **12**, 521 (2019).

737 [88] Tzourio-Mazoyer, N. *et al.* Automated anatomical labeling of activations in SPM using a
738 macroscopic anatomical parcellation of the MNI MRI single-subject brain. *NeuroImage* **15**,
739 273–289 (2002).

740 [89] Sperr, E. PubMed by Year (2022). URL <https://esperr.github.io/pubmed-by-year/>.

741 [90] Avants, B. B. *et al.* The optimal template effect in hippocampus studies of diseased popula-
742 tions. *NeuroImage* **49**, 2457–2466 (2010). URL <https://linkinghub.elsevier.com/retrieve/pii/S1053811909010611>.

743

Materials and Methods

744

745 **Human Dataset** MRI data was collected from forty-one individuals, including thirteen healthy controls and twenty-eight drug-resistant
746 epilepsy patients at the Hospital of the University of Pennsylvania. Twenty-four patients underwent stereoelectroencephalography
747 (SEEG) implantation and four underwent electrocorticography (ECoG) implantation. Ten of the SEEG patients had clinically
748 annotated seizures and were used for SFC analyses. Inclusion criteria consisted of all individuals who agreed to participate in our research
749 scanning protocol, and (if they had implantations) allowed their de-identified intracranial EEG (iEEG) data to be publicly available
750 for research purposes on the International Epilepsy Electrophysiology Portal (<https://www.ieeg.org>)^{68,69}. Seizure evaluation was
751 determined via comprehensive clinical assessment, which included
752

753

754

755

756

757

758

759

760 multimodal imaging, scalp and intracranial video-EEG monitoring,
761 and neuropsychological testing. This study was approved by the
762 Institutional Review Board of the University of Pennsylvania, and
763 all subjects provided written informed consent prior to participating.
764 See [Table S2](#) for subject demographics.

765 **Structure** Methods and pipelines for structural connectivity genera-
766 tion and analysis are described in the following sections. Specific
767 GitHub files and code are included where applicable.

768 **Imaging Protocol** Prior to electrode implantation, MRI data were
769 collected on a 3T Siemens Magnetom Trio scanner using a 32-
770 channel phased-array head coil. High-resolution anatomical images
771 were acquired using a magnetization prepared rapid gradient echo
(MPRAGE) T1-weighted sequence (repetition time = 1810 ms, echo
772 time = 3.51ms, flip angle = 9, field of view = 240mm, resolution =
773 0.94x0.94x1.0 mm³). High Angular Resolution Diffusion Imaging
774 (HARDI) was acquired with a single-shot EPI multi-shell diffusion-
775 weighted imaging (DWI) sequence (116 diffusion sampling directions,
776 b-values of 0, 300, 700, and 2000s/mm², resolution = 2.5x2.5x2.5
777 mm³, field of view = 240mm). Following electrode implantation,
778 spiral CT images (Siemens) were obtained clinically for the pur-
779 poses of electrode localization. Both bone and tissue windows were
780 obtained (120kV, 300mA, axial slice thickness = 1.0mm)

781 **Diffusion Weighted Imaging (DWI) Preprocessing** HARDI images
782 were subject to the preprocessing pipeline, QSIPrep, to ensure
783 reproducibility and implementation of the best practices for pro-
784 cessing of diffusion images⁷⁰. Briefly, QSIPrep performs advanced
785 reconstruction and tractography methods in curated workflows us-
786 ing tools from leading software packages, including FSL, ANTs, and
787 DSI Studio with input data specified in the Brain Imaging Data
788 Structure (BIDS) layout.

789 **Structural Network Generation** DSI-Studio ([http://dsi-
790 studio.labsolver.org](http://dsi-studio.labsolver.org), version: December 2020) was used to
791 reconstruct the orientation density functions within each voxel
792 using generalized q-sample imaging with a diffusion sampling
793 length ratio of 1.25⁷¹. Deterministic whole-brain fiber tracking
794 was performed using an angular threshold of 35 degrees, step size
795 of 1mm, and quantitative anisotropy threshold based on Otsu's
796 threshold⁷². Tracks with length shorter than 10mm or longer than
797 800mm were discarded, and a total of 1,000,000 tracts were gener-
798 ated per brain. Deterministic tractography was chosen based upon
799 prior work indicating that deterministic tractography generates
800 fewer false positive connections than probabilistic approaches, and
801 that network-based estimations are substantially less accurate
802 when false positives are introduced into the network compared
803 with false negatives³⁰. To calculate structural connectivity,
804 atlases listed in [Table 1](#) were used. Structural networks were
805 generated by computing the number of streamlines passing through
806 each pair of structural regions in each specific atlas. Streamline
807 counts were log-transformed and normalized to the maximum
808 streamline count, as is common in prior studies^{24,73-75}. GitHub:
809 packages/imaging/tractography/tractography.py

810 **Atlases** Atlas descriptions and sources used in this study are found
811 in [Table S1](#). The 55 atlases used are listed explicitly in the reporting
812 of effect sizes in [Fig. 7d](#). All atlases were sourced in MNI space
813 and if not already, resliced to dimensions 182x218x182. Atlases
814 were linear and non-linear registered to T1w subject space using
815 the ICBM 2009c Nonlinear Asymmetric template⁷⁶ and FSL flirt
816 and fnirt⁷⁷.

817 We also included three atlases registered using surface-based
818 approaches. These atlases (the DKT, DK, and Destrieux atlases) are
819 output from FreeSurfer's recon-all pipeline⁷⁸. Many neuroimaging
820 studies and software use volumetric approaches for registration²¹,
821 yet surface-based approaches may yield more accurate labeling of
822 the cortical surface ([Fig. S6](#)). The DKT40 atlas referred in this
823 study is the surface version, while the DKT31 OASIS is the publicly
824 available volumetric version (see [Table S1](#)).

825 In addition to published standard atlases above, we used whole-
826 brain random atlases. A limitation of standard atlases is that they
827 may not have anatomical definitions for all regions of the brain, and

828 therefore, implanted electrodes may not be assigned properly to a
829 region. This limitation was the impetus of our study (i.e., selecting
830 an appropriate atlas for SEEG electrode localization and quantifying
831 SFC). Whole-brain random atlases, in contrast, provide coverage to
832 all implanted electrodes. They allow for the ability to change some
833 morphological properties (i.e. parcellation size), while keeping other
834 morphologies the same (e.g., parcellation shape; [Fig. 2d](#)). However,
835 a limitation of random atlases is that their regions may not represent
836 true anatomical or functional boundaries. Random atlases were
837 built in the ICBM 2009c Nonlinear Asymmetric template space
838 and covered all voxels, excluding those labeled as CSF or outside
839 the brain. To fill these points, a pseudo grassfire algorithm was
840 applied³⁰. Briefly, N points representing the number of parcels of
841 the atlas were randomly chosen as seed points. These seed points
842 were iteratively expanded in all six Cartesian directions until all
843 points were covered by one of the initial N seeds. After each iterative
844 step, the smallest volume region expanded first. Random atlases
845 created were of N equal to 10, 30, 50, 75, 100, 200, 300, 400, 500,
846 750, 1000, 2000, 5000, and 10000 parcels. Five permutations for
847 each N were created. GitHub code to generate random atlases:
848 packages/imaging/randomAtlas/randomAtlasGeneration.py
849

850 **Atlas Morphology: Volume and Sphericity** Atlas morphological mea-
851 surements included parcellation size (volume) and shape (sphericity)
852 ([Fig. 2](#)). Parcellation volume was calculated as the number of voxels
853 in an parcel and log10 transformed. Parcellation sphericity was
854 calculated as the ratio of the surface area of a sphere with an equal
855 volume of the parcellation to the actual surface area of the atlas
856 parcellation. Under this definition, sphericity is bounded from 0 to
857 1 where 1 is a perfect sphere. For reference, a perfect cube and a
858 hemi-sphere have a sphericity of 0.8 and 0.7 respectively. GitHub:
859 packages/imaging/regionMorphology/regionMorphology.py
860

861 **Structural Network Measures** We characterized the structural net-
862 work topology of 52 atlases ([Fig. 3](#) and [Fig. S3](#)). The three surface-
863 based atlases (DKT40, DK, and Destrieux atlases output from
864 the FreeSurfer recon-all pipeline⁷⁸) were excluded from analyses of
865 [Fig. 2](#) and [Fig. 3](#) because they were individually registered to each
866 subjects' T1w image. To quantify network topology, we examined
867 density, mean degree, mean clustering coefficient, characteristic
868 path length, and small worldness. Connectivity matrices were
869 first binarized, using a threshold of 0, and a distance matrix was
870 computed. The same binarization process and threshold was used
871 across all atlases. The distance of any nodes that were discon-
872 nected from the main graph was set to the maximum distance
873 between any pair of nodes in the main graph. Density, mean de-
874 gree, clustering coefficient, and characteristic path length were then
875 calculated on the binary, undirected graphs. Small worldness was
876 calculated as the σ -ratio where $\sigma = \gamma/\lambda$ and γ is the ratio of the
877 average, normalized clustering coefficient, C, to the normalized
878 characteristic path length, I. $\gamma = CG/CR$ and $\lambda = LG/IR$ where G
879 is the graph of interest and R represents a 'random' graph that is
880 equivalent to G. To approximate the equivalent random graph R
881 due to intractable computational costs⁷⁹, a well-known analytical
882 equivalent $CR = d/N$ and $IR = \log N/\log d$ were used, where d
883 denotes average nodal degree. All network measures were calculated
884 using the [Brain Connectivity Toolbox for Python](#). GitHub: pa-
885 pers/brainAtlas/Script_05_structure_02_network_measures.py
886

887 **Function** Methods and pipelines for functional connectivity genera-
888 tion and analysis are described in the following sections. Specific
889 GitHub files and code are included where applicable.

890 **Intracranial EEG Acquisition** Stereotactic Depth Electrodes were im-
891 planted in patients based on clinical necessity. Continuous SEEG
892 signals were obtained for the duration of each patient's stay in
893 the epilepsy monitoring unit. Intracranial data was recorded at
894 either 512 or 1024 Hz for each patient. Seizure onset times were
895 defined by the unequivocal onset⁸⁰. All annotations were verified
896 and consistent with detailed clinical documentation. If a patient
897 had more than one seizure annotated, the first seizure longer than
898 30 seconds without artifacts was used.

897 **Electrode Localization** In-house software⁸¹ was used to assist in
898 localizing electrodes after registration of pre-implant and post-
899 implant neuroimaging data. All electrode coordinates and labels
900 were saved and matched with the electrode names on IEEG.org.
901 All electrode localizations were verified by a board-certified neu-
902 roradiologist (J.S.). Electrode contact assignment to atlas region
903 assignment was performed by rounding electrode coordinates (x,y,z)
904 to the nearest voxel and indexing the given atlas at that voxel in
905 the same space as the patient's T1w image. Electrodes that fell
906 outside the atlas of interest were excluded from subsequent analysis.
907 Please see Fig. S10 for visualization. We also show the percent-
908 age of contacts assigned a region given an atlas (Fig. S7) GitHub:
909 packages/atlasLocalization/atlasLocalization.py

910 **Functional Connectivity Network Generation** Functional connectivity
911 networks were generated from four periods: interictal, preictal, ictal,
912 and postictal. (1) The interictal period consisted of the time ap-
913 proximately 6 hours before the ictal period. (2) The preictal period
914 consisted of the time immediately before the ictal period. (3) The
915 ictal period consisted of the time between the seizure unequivocal
916 onset and seizure termination. (4) The postictal period consisted of
917 the time immediately after the ictal period. Interictal, preictal, and
918 postictal periods were 180 seconds in duration. Following removal
919 of artifact-ridden electrodes, SEEG signals inside either GM or WM
920 for each period were common-average referenced to reduce potential
921 sources of correlated noise⁸². Next, each period was divided into
922 2s time windows with 1s overlap⁸³⁻⁸⁶. To generate a functional
923 network representing broadband functional interactions between
924 SEEG signals (Fig. 4b), we carried out a method described in detail
925 previously^{13,85}. Namely, signals were notch-filtered at 60 Hz to
926 remove power line noise, low-pass and high-pass filtered at 127 Hz
927 and 1Hz to account for noise and drift, and pre-whitened using a
928 first-order autoregressive model to account for slow dynamics. Func-
929 tional networks were then generated by applying a normalized cross
930 correlation function ρ between the signals of each pair of electrodes
931 within each time window, using the formula:

$$\rho_{xy} = \max_{\tau} \left[\frac{1}{T} \sum_{t=1}^T \frac{[x_k(t) - \bar{x}_k] * [y_k(t + \tau) - \bar{y}_k]}{\sigma_{x_k} \sigma_{y_k}} \right]$$

932 where x and y are signals from two electrodes, k is the 2s time
933 window, t is one of the T samples during the time window, and
934 τ is the time lag between signals, with a maximum lag of 0.5
935 s. Here, σ represents the standard deviation of the signal. Note
936 that functional connectivity measurements were also calculated for
937 coherence and zero time-lag Pearson and Spearman rank correlations
938 with associated p-values in defined frequency bands reviewed in
939 Newson and Thiagarajan 2019⁸⁷, but were not analyzed or used in
940 hypothesis testing in the study. For data, available data, please see
941 "Data availability and Reproducibility" section below. Networks are
942 represented as fully-weighted connectivity matrices. GitHub Code:
943 GitHub: code/tools/echobase.py

944 **Structure-Function Correlation** To quantify the relationship between
945 structure and function in the epileptic brain, we computed the Spear-
946 man rank correlation coefficient between the edges of the structural
947 connectivity network and the edges of the functional connectivity
948 networks (Fig. 4c). To avoid redundancy given the symmetric nature
949 of the matrices, only the upper triangle was analyzed. In brief, the
950 structural connectivity network, representing normalized streamline
951 counts between each atlas region, was first down sampled to only
952 include regions that contained at least one SEEG contact Fig. S10.
953 This gave one static representation of structural connectivity. In
954 the case where multiple electrodes fell in the same atlas region, a
955 random electrode was selected to represent the functional activity of
956 that neuroanatomically defined region. Next, for every time-window
957 of the functional network, the functional network edges were corre-
958 lated with the down sampled, static structural network edges. This
959 resulted in a structure-function correlation time series. Note that
960 atlases with very small region volumes included more electrodes for
961 SFC calculation. Electrodes that did not localize to an atlas were
962 excluded from analysis. To average the SFC for all patients and
963 each atlas (Fig. 5), SFC time-series was resampled to 100 seconds

964 for each period and each sample was averaged together. GitHub
965 code: packages/eeg/echobase/echobase.py
966

967 **rsSFC and Δ SFC** Resting-state SFC (rsSFC) was defined as the SFC
968 during the interictal period, approximately 6 hours before the ictal
969 period. The mean SFC of that period was computed. Δ SFC was
970 defined as the change in the mean SFC from the preictal to the ictal
971 period (Fig. 5 top left panel). rsSFC and Δ SFC was calculated for
972 each atlas (Fig. 6).

973 **Statistics** Preictal and ictal SFC for each atlas were compared using
974 effect sizes across the 55 atlases shown in Fig. 6d. Cohen's d and
975 the difference between preictal and ictal SFC was calculated.

976 **Data availability and Reproducibility** All code
977 files used in this manuscript are available at
978 <https://github.com/andyrevell/revellLab>. All de-identified
979 raw and processed data (except for patient MRI imaging) are
980 available for download by following the links on the GitHub.
981 Raw imaging data is available upon reasonable request from
982 Principal Investigator K.A.D. iEEG snippets used specifically in
983 this manuscript are also available, while full iEEG recordings
984 are publicly available at <https://www.ieeg.org>. The Python
985 environment for the exact packages and versions used in this study
986 are contained in the environment directory within the GitHub. The
987 QSHIPprep docker container was used for DWI preprocessing.

Acknowledgements

988 We thank Adam Gibson, Carolyn Wilkinson, Jacqueline Boccanfuso,
989 Magda Wernovsky, Ryan Archer, Kelly Oechsel, members of
990 Andrew's Thesis Committee, and all other members and staff of the
991 Center for Neuroengineering and Therapeutics for their continued
992 help and support in this work.

Funding

993 This work was supported by National Institutes of Health grants 5-
994 T32-NS-091006-07, 1R01NS116504, 1R01NS099348, 1R01NS085211,
995 and 1R01MH112847. We also acknowledge support by the Thornton
996 Foundation, the Mirowski Family Foundation, the ISI Foundation,
997 the John D. and Catherine T. MacArthur Foundation, the Sloan
998 Foundation, the Pennsylvania Tobacco Fund, and the Paul Allen
999 Foundation.

Competing Interests

1000 The authors declare no competing interests.

1001

1004 **Supplementary Material**

1005 Please see supplemental figures and tables contained below.

- 1006 • Figures
 - 1007 – [Fig. S1](#): Atlas, Template, and Coordinate (Stereotactic) 1062 Space
 - 1008 – [Fig. S2](#): Atlas Morphology: Sizes and Shapes (All atlases) 1063
 - 1009 – [Fig. S3](#): Network measures for remaining atlases 1064
 - 1010 – [Fig. S4](#): Network measures for controls and patients 1065 separated
 - 1011 – [Fig. S5](#): Network measures for different thresholds 1066
 - 1012 – [Fig. S6](#): Effects of Registration: Volumetric- and Surface- 1067 based approaches
 - 1013 – [Fig. S7](#): Coverage of electrode contacts 1068
 - 1014 – [Fig. S8](#): "Brain Atlas" Search in PubMed 1069
 - 1015 – [Fig. S9](#): Prevalence of select brain atlases and neuroimaging 1070 software
 - 1016 – [Fig. S10](#): Electrode localization and region selection 1071
- 1021 • Tables
 - 1022 – [Table. S1](#): Atlas Sources and References (3 pages). 1072
 - 1023 – [Table. S2](#): Patient and Control Demographics 1073
- 1024 • Other materials
 - 1025 – [Glossary](#)

1026 **Glossary**

- 1027 1. **Atlas abbreviations and definitions.** For further details, 1028 see [Table. S1](#).
 - 1029 (a) **AAL.** Automated anatomical labeling atlas.
 - 1030 (b) **AAL1, AAL2, AAL3.** AAL atlas versions 1, 2, and 3, 1031 respectively.
 - 1032 (c) **AAL-JHU.** The AAL atlas and the JHU labels atlas 1033 combined. For overlapping regions, the JHU atlas takes 1034 precedence.
 - 1035 (d) **AAL600.** AAL atlas with 600 parcels.
 - 1036 (e) **AICHA.** Atlas of Intrinsic Connectivity of Homotopic 1037 Areas.
 - 1038 (f) **BNA.** Brainnetome atlas.
 - 1039 (g) **Craddock 200-400.** Craddock atlases with a specified 1040 number of parcels (e.g. Craddock 200 will have 200 1041 parcels). There are two atlas sizes publicly available - 1042 the Craddock 200 and Craddock 400 atlases.
 - 1043 (h) **DKT31 OASIS.** The DKT atlas from the OASIS 1044 dataset. See [Table. S1](#) sources for more details. It is 1045 the volumetric version.
 - 1046 (i) **DKT40.** The DKT atlas used as part of FreeSurfer. 1047 See [Table. S1](#) sources for more details. It is the surface 1048 version.
 - 1049 (j) **DK.** The Desikan-Killiany atlas. Surface atlas from 1050 FreeSurfer.
 - 1051 (k) **HO.** Harvard-Oxford atlas.
 - 1052 (l) **HO cortical-only.** HO atlas with only cortical regions. 1053 The symmetrical regions (the same region name on the 1054 contralateral hemisphere) are labeled with *different* 1055 identifications. Thus, this atlas has *non-symmetrical* 1056 labels (e.g. both temporal pole regions are labeled with a 1057 different identification number). Left and right structures 1058 were re-labeled with different identification numbers using the 1059 sagittal mid-line (in MNI space, x coordinate at zero) as 1060 a separator.
 - 1061 (m) **HO cort-only.** Same as the HO cortical-only atlas.
- 1062 (n) **HO sym. cortical only.** HO atlas with only cortical 1063 regions. The symmetrical regions (the same region name 1064 on the contralateral hemisphere) are labeled with the 1065 *same* identification. Thus, this atlas is has *symmetrical* 1066 labels (e.g. both temporal pole regions are labeled with 1067 the same identification number). The default atlases 1068 given by FSL are symmetrical atlases.
- 1069 (o) **HO subcortical-only.** HO atlas with only subcortical 1070 regions.
- 1071 (p) **HO subcort-only.** Same as the HO subcortical-only 1072 atlas.
- 1073 (q) **HO combined.** HO atlas with both cortical and sub- 1074 cortical regions. This atlas has non-symmetrical labeling 1075 (e.g. both temporal pole regions are labeled with a differ- 1076 ent identification number).
- 1077 (r) **HO cortical + subcortical.** Same as the HO combined 1078 atlas.
- 1079 (s) **JHU.** The Johns Hopkins University atlases. There are 1080 two white matter atlases: the JHU labels and JHU 1081 tracts atlases.
- 1082 (t) **MMP.** Multi-modal parcellation atlas. Sometimes re- 1083 ferred to as the "Glasser Atlas" after the first author of 1084 the original publication.
- 1085 (u) **Random atlas 10-10,000.** Atlases created with ran- 1086 dom parcels with a specified number of parcels (e.g. Ran- 1087 dom atlas 1,000 will have 1,000 parcels). These atlases 1088 were built in the ICBM 2009c Nonlinear Asymmetric 1089 template. Thus, these atlases are whole-brain atlases 1090 (includes cortical gray matter, subcortical gray matter, 1091 and white matter). See the 'Atlases' Methods section for 1092 more details.
- 1093 (v) **Schaefer 100-1,000.** The Schaefer atlases with a speci- 1094 fied number of parcels (e.g. Schaefer 100 will have 100 1095 parcels). There are ten atlases of 100, 200, 300, 400, 500, 1096 600, 700, 800, 900, and 1,000 parcels.
- 1097 (w) **Yeo liberal.** The Yeo atlases where the boundaries of 1098 each parcel is extended slightly into the white matter, 1099 past the cortical boundary.
- 1100 (x) **Yeo conservative.** The Yeo atlases where the bound- 1101aries of each parcel is extended slightly into the white 1102 matter, past the cortical boundary.
- 1103 2. **Δ SFC.** The change in SFC between ictal and preictal stats 1104 ($SFC_{ictal} - SFC_{preictal}$). This indicates whether or not the 1105 change in functional connectivity is congruent with the 1106 underlying structural connectivity.
- 1107 3. **Contact.** A single sensor on an electrode that records LFP. 1108 Not to be confused with an electrode. See [Fig. S7](#), bottom.
- 1109 4. **ECOG:** Electrocorticography.
- 1110 5. **Electrode.** Not to be confused with contact. See [Fig. S7](#), 1111 bottom.
- 1112 6. **Derived atlas:** An atlas which was derived from another 1113 atlas. For example, the AAL 600 is derived from the AAL 1114 atlas in which its parcellations are further sub-divided using a 1115 specified algorithm. Derived atlases may also be sub-divided 1116 randomly so that it is both considered a random and derived 1117 atlas (a quasi-random atlas). The BNA is also a derived atlas 1118 in which it initially used the parcellations of the DK atlas.
- 1119 7. **Functional connectivity (FC).** The statistical relationship 1120 between two signals (two contacts in this study).
- 1121 8. **grayordinate.** Atlas that includes gray matter structures, 1122 including cortical and subcortical gray matter regions.
- 1123 9. **ROI.** Region of interest
- 1124 10. **ROI, parcel, parcellation, region.** These terms may be 1125 used interchangeably in the literature. They refer to discrete 1126 areas of a brain. These regions are labeled with a categorical 1127 identification (rather than a continuous variable seen in tem- 1128 plates - see [Fig. S1](#)), and all voxels or surface vertices with the 1129 same identification are part of the same region.

1130 11. **SEEG**: Stereoelectroencephalography.
1131 12. **Structural connectivity (SC)**. The physical relationship
1132 between two brain regions. We use streamline counts in this
1133 manuscript from High Angular Resolution Diffusion Imaging.
1134 13. **T1w**. T1-weighted MRI image.

Clarifying Terminologies

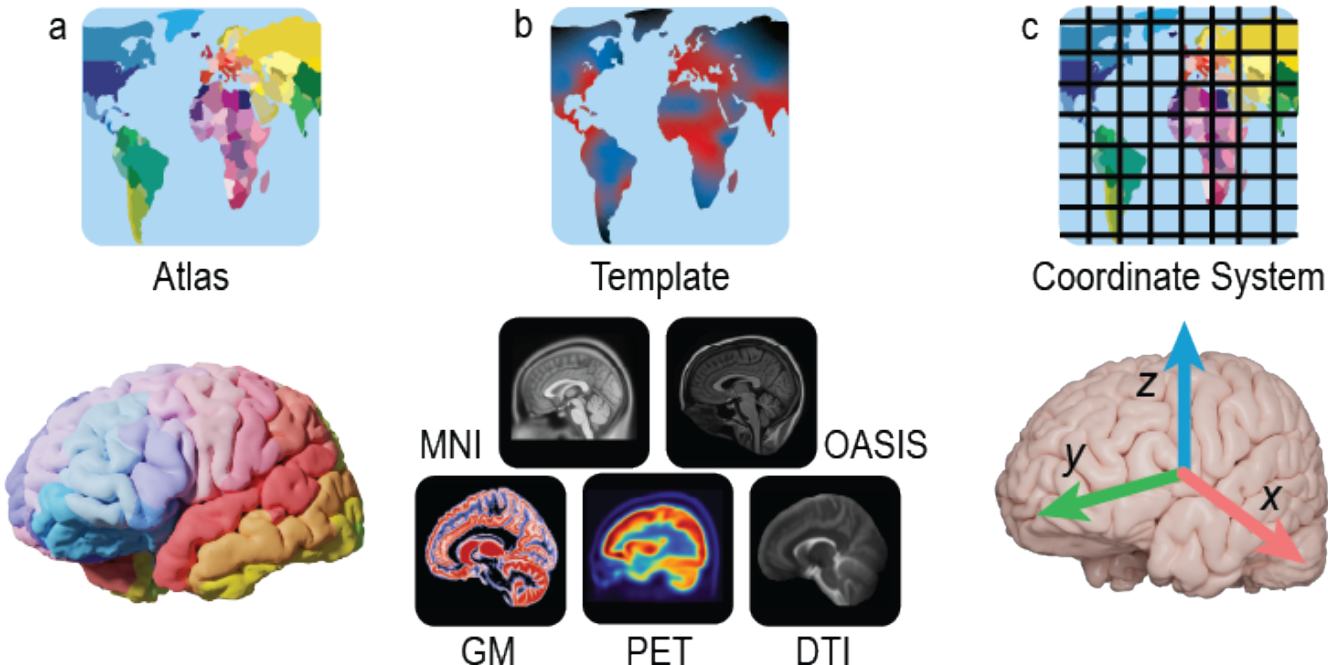


Fig. S1. Atlas, Template, and Coordinate (Stereotactic) Space. | These three terms are commonly confused in the neuroscience literature because they all relate to the "map" of the brain. "Atlas" and "template" are sometimes used interchangeably³, however, they are distinct. Here, we define them more formally. **a**, A brain **atlas** refers to a neurological map that defines brain region *labels*. We use this definition throughout the main text. **b**, An atlas is distinct from a brain **template**, which refers to a brain *pattern*. Similar in common usage, a template is a mold, gauge, or starting point representation of the brain. Usually it is composed of multiple individuals' brain representing an average of a population. Many templates exist and are reviewed in various publications^{2,9}. The templates illustrated here are the MNI152 Nonlinear asymmetric 2009c T1w template (<http://www.bic.mni.mcgill.ca>), the OASIS brain template <https://www.oasis-brains.org/> created and used by ANTs (<http://stnava.github.io/ANTs/> with templates linked here), a gray matter probability map, a PET template, and a b0 DTI template. **c**, The coordinate system, or the **stereotactic space**, of the brain describes the physical positioning of the brain, similar to the geographical coordinate system of longitude and latitude of the Earth. Historically, a common stereotactic space was the Talairach space, and more recently, the MNI spaces. The analogy between the geographical terms of the Earth and the geographical terms of the brain is not exact. The analogy falls apart in that while there is one world, there are many brains. There is variability across populations and a spectrum of differences between species, therefore, it is challenging to represent one brain for use in every scientific study appropriately. **MNI**, Montreal Neurological Institute; **OASIS**, Open Access Series of Imaging Studies; **GM**, Gray Matter probability map; **PET**, Positron Emission Tomography; **DTI**, Diffusion Tensor Imaging.

Please see the end of this document for a high-resolution, highlightable version

Atlas	Source	Note	Reference(s)
AAL	1	AAL1. The successor to the Talairach atlas. The goal was to reduce confusion in relating stereotaxic space (a set of brain coordinates) and anatomical labels. It is based on a single individual (the Collin-27 template) and it is not a probabilistic map. The Collin-27 template was intended for segmentation, and not stereotaxy; it did not capture anatomical variability. However, the high resolution in 1998 proved attractive to research groups.	(1) Tzourio-Mazoyer, N. et al. Automated Anatomical Labeling of Activations in SPM Using a Macroscopic Anatomical Parcellation of the MNI MRI Single-Subject Brain. <i>NeuroImage</i> 15, 273–289 (2002). (2) Collin-27 template: Holmes, C. J. et al. Enhancement of MR Images Using Registration for Signal Averaging: <i>Journal of Computer Assisted Tomography</i> 22, 324–333 (1998). (3) Website about Collin-27: https://www.bic.mni.mcgill.ca/ServicesAtlases/Colin27
	2	AAL2: new parcellation of orbitofrontal cortex. AAL1 orbitofrontal cortex was parcellated according to a French publication by Jules Déjerine in 1895. Chiavaras and Petrides (2000) proposed another parcellation of the orbital surface allowing for the comparison of human frontal lobe anatomy with that of macaques.	(1) Rolls, E. T., Joliot, M. & Tzourio-Mazoyer, N. Implementation of a new parcellation of the orbitofrontal cortex in the automated anatomical labeling atlas. <i>NeuroImage</i> 122, 1–5 (2015). (2) Chiavaras, M. M. & Petrides, M. Orbitofrontal sulci of the human and macaque monkey brain. <i>The Journal of Comparative Neurology</i> 422, 35–54 (3) Déjerine, J. <i>Anatomie des centres nerveux</i> . (Rueff Paris, 1895).
	3	AAL3: new parcellations - anterior cingulate, thalamus, nucleus accumbens, substantia nigra, ventral tegmental area, red nucleus, locus coeruleus, and raphe nuclei. 2019. AAL3v1: changes of thalamus in line with FreeSurfer 7. 2020.	Rolls, E. T., Huang, C.-C., Lin, C.-P., Feng, J. & Joliot, M. Automated anatomical labelling atlas 3. <i>NeuroImage</i> 206, 116189 (2020).
	4	Website for download - group that made AAL toolbox and user guides.	https://www.gin.cnrs.fr/en/tools/aal/
	5	SPM - software compatible with AAL toolbox. Generally, designed for the analysis of brain imaging data sequences. Extensions include AAL toolbox.	(1) Statistical parametric mapping: the analysis of functional brain images. (Elsevier/Academic Press, 2007). (2) Website: https://www.fil.ion.ucl.ac.uk/spm/ext/
	6	AAL 600 - Subparcellations of the AAL atlas into 600 subregions. Upsampling algorithm described. Part of larger framework for evaluating the effect of parcellation scale.	Bassett, D. S., Brown, J. A., Deshpande, V., Carlson, J. M. & Grafton, S. T. Conserved and variable architecture of human white matter connectivity. <i>NeuroImage</i> 54, 1262–1279 (2011)
	7	Use cases of AAL600. Both Ashourvan et al. (2017) and Hermundstad et al. (2014) use AAL600 for generating both structural and functional connectivity networks.	(1) Ashourvan, A., Telesford, Q. K., Verstynen, T., Vettel, J. M. & Bassett, D. S. Multi-scale detection of hierarchical community architecture in structural and functional brain networks. (2017) (2) Hermundstad, A. M. et al. Structurally-Constrained Relationships between Cognitive States in the Human Brain. <i>PLoS Comput Biol</i> 10, e1003591 (2014).
AICHA	8	AICHA tries to account for <i>homotopy</i> : the concept that each region in one hemisphere has a homologue in the other.	Joliot, M. et al. AICHA: An atlas of intrinsic connectivity of homotopic areas. <i>Journal of Neuroscience Methods</i> 254, 46–59 (2015)
Brainnetome	9	Connectivity-based atlas. Further subdivision of structural parcellations using the DK (Desikan-Killiany) protocol, with adjustments.	Fan, L. et al. The Human Brainnetome Atlas: A New Brain Atlas Based on Connec-tional Architecture. <i>Cerebral cortex</i> (New York, N.Y. : 1991) 26, 3508–26 (2016). Website: http://atlas.brainnetome.org
	10	DSI studio created by Fang-Cheng (Frank) Yeh. Many reconstruction and tracking algorithms are published and incorporated into DSI Studio. See citations page on website. Many atlases available, including Brainnetome. Can use custom atlas.	(1) Website: http://dsi-studio.labsolver.org/ (2) Example of reconstruction method: Fang-Cheng Yeh, Wedeen, V. J. & Tseng, W.-Y. I. Generalized q-Sampling Imaging. <i>IEEE Trans. Med. Imaging</i> 29, 1626–1635 (2010).
Brodmann	11	Perspective, description, and historical significance of Korbinian Brodmann's map.	Zilles, K. & Amunts, K. Centenary of Brodmann's map — conception and fate. <i>Nat Rev Neurosci</i> 11, 139–145 (2010)
	12	References to the original German and English translation provided.	(1) Original German: <i>Vergleichende Lokalisationslehre der Grosshirnrinde in ihren Prinzipien dargestellt auf Grund des Zellenbaues</i> . (1909) (2) English translation: Brodmann, K. & Gary, L. J. Brodmann's localisation in the cerebral cortex: the principles of comparative localisation in the cerebral cortex based on cytoarchitectonics. (Springer, 2006)
	13	The atlas is available through MRIcro, a legacy tool developed by Chris Rorden (University of South Carolina). The atlas is based on work from the Van Essen lab (Washington University in St. Louis) with corresponding Talairach coordinates, and transformed by Krish Singh (Cardiff University) to MNI space.	(1) Chris Rorden legacy tools webpage: https://people.cas.sc.edu/rorden/ (2) Updated webpage: https://crl.readthedocs.io/ (3) About Brodmann atlas: https://people.cas.sc.edu/rorden/micro/lesion.html (4) BALSA: https://balsa.wustl.edu/Wz8r
CerebrA	14	Introduction to the CerebrA and MNI-ICBM2009c average brain template.	Manera, A. L., Dadar, M., Fonov, V. & Collins, D. L. CerebrA, registration and manual label correction of Mindboggle-101 atlas for MNI-ICBM152 template. <i>Sci Data</i> 7, 237 (2020). Website: https://doi.gin.g-node.org/10.12751/g-node.be5e62
Craddock	15	Original publication about functional parcellations.	Craddock, R. C., James, G. A., Holtzheimer, P. E., Hu, X. P. & Mayberg, H. S. A whole brain fMRI atlas generated via spatially constrained spectral clustering. <i>Hum. Brain Mapp.</i> 33, 1914–1928 (2012).
	16	GitHub with source code to make atlas with N clusters.	GitHub: http://ccraddock.github.io/cluster_roi/atlas.html
	17	Publicly available pre-made atlases at N=200 and N=400 from ABIDE (Autism Brain Imaging Data Exchange), co-founded by Cameron Craddock. 4x4x4mm resolution.	ABIDE: http://preprocessed-connectomes-project.org/abide/Pipelines.html

Table S1. Atlas sources and references. | This table provides a short note and references to the source material of common atlases in the neuroscience literature. See also [Table 1](#).

Please see the end of this document for a high-resolution, highlightable version

Atlas	Source	Note	Reference(s)
DKT	18	Original DKT protocol and atlas. A protocol for an atlas is a set of instructions for how the brain should be labeled. See AAL, Hammersmith, Harvard-Oxford, and JHU atlases.	Desikan, R. S. et al. An automated labeling system for subdividing the human cerebral cortex on MRI scans into gyral based regions of interest. <i>NeuroImage</i> 31, 968–980 (2006).
	19	DKT protocol, Mindboggle-101 dataset, and atlas creation.	Klein, A. & Tourville, J. 101 Labeled Brain Images and a Consistent Human Cortical Labeling Protocol. <i>Front. Neurosci.</i> 6, (2012).
	20	Summary of Mindboggle project, history, atlas development, applications, and current problems.	Klein, A. et al. Mindboggling morphometry of human brains. <i>PLoS Comput Biol</i> 13, e1005350 (2017)
	21	Websites for downloading data including the labeled brains and atlases.	Open Science Framework: https://osf.io/nhtur/ Harvard Dataverse: https://dataVERSE.harvard.edu/dataVERSE/mindboggle Labels: https://mindboggle.readthedocs.io/en/latest/labels.html GitHub: https://github.com/nipy/mindboggle
	22	Subcortical regions.	http://www.neuromorphometrics.com/
	23	FreeSurfer.	https://surfer.nmr.mgh.harvard.edu/
Destrieux	24	Original article describes automatic labeling algorithm from probabilistic information using a manually labeled training set. 74 parcellations per hemisphere (excluding subcortical structures). Available in FreeSurfer with subcortical structures output.	(1) Destrieux, C., et al., E. Automatic parcellation of human cortical gyri and sulci using standard anatomical nomenclature. <i>NeuroImage</i> 53, 1–15 (2010). (2) Fischl, B. Automatically Parcellating the Human Cerebral Cortex. <i>Cerebral Cortex</i> 14, 11–22 (2004).
	25	FreeSurfer information on atlases available.	(1) https://surfer.nmr.mgh.harvard.edu/fswiki/CorticalParcellation (2) https://surfer.nmr.mgh.harvard.edu/fswiki/DestrieuxAtlasChanges
Gordon-Petersen	26	Original article.	Gordon, E. M. et al. Generation and Evaluation of a Cortical Area Parcellation from Resting-State Correlations. <i>Cereb. Cortex</i> 26, 288–303 (2016).
	27	Resource to download atlas.	https://sites.wustl.edu/petersenschlaggarlab/resources/
Hammersmith	28	Original article (for regions 1-49), including their Hammersmith protocol (or “algorithm”).	Hammers, A. et al. Three-dimensional maximum probability atlas of the human brain, with particular reference to the temporal lobe. <i>Hum. Brain Mapp.</i> 19, 224–247 (2003).
	29	Updated regions (for regions 50-83).	Gousias, I. S. et al. Automatic segmentation of brain MRIs of 2-year-olds into 83 regions of interest. <i>NeuroImage</i> 40, 672–684 (2008).
	30	Download atlas with 83 regions.	http://brain-development.org/brain-atlases/adult-brain-atlases/adult-brain-maximum-probability-map-hammersmith-atlas-n30r83-in-mni-space/
Harvard-Oxford	31	Atlas developed at the Center for Morphometric Analysis (CMA) at Massachusetts General Hospital and distributed with FSL.	https://fsl.fmrib.ox.ac.uk/fsl/fslwiki/Atlases
	32	Individual segmentations were segmented by CMA using in-house software. Probability maps were then created. Freesurfer link (right) has archived CMA’s website and contains the Harvard-Oxford labeling protocols.	FreeSurfer description about CMA: http://freesurfer.net/fswiki/CMA Link to website archive: https://web.archive.org/web/20180413052010/http://www.cma.mgh.harvard.edu/
JHU	33	JHU labels: Protocol to reconstruct eleven white matter tracts and their segmentation into ROI labels. Included in FSL.	Wakana, S. et al. Reproducibility of quantitative tractography methods applied to cerebral white matter. <i>NeuroImage</i> 36, 630–644 (2007).
	34	JHU Tracts: white matter parcellation atlas based on DTI probabilistic tractography of 11 major white matter tracts. Protocol defining manually identified ROIs from which the tracts were formed are described in Wakana et al. (2005). Included in FSL.	Hua, K. et al. Tract probability maps in stereotaxic spaces: Analyses of white matter anatomy and tract-specific quantification. <i>NeuroImage</i> 39, 336–347 (2008).
	35	Textbook with more information about these atlases.	MRI atlas of human white matter. (Elsevier, Acad. Press, 2011).
Julich	36	Cytoarchitecture map. Successor to both the Brodmann and Eickhoff-Zilles atlases. The Eichhoff-Zilles is an SPM toolbox (see note 5 about the AAL atlas) for probabilistic cytoarchitecture.	(1) Amunts, K., Mohlberg, H., Bludau, S., & Zilles, K. Julich-Brain: A 3D probabilistic atlas of the human brain’s cytoarchitecture. 6 (2020). (2) Eickhoff, S. B. et al. A new SPM toolbox for combining probabilistic cytoarchitectonic maps and functional imaging data. <i>NeuroImage</i> 25, 1325–1335 (2005)
	37	Website for the Julich Atlas and SPM toolbox.	https://www.fz-juelich.de/inn/inn-1/DE/Forschung/_docs/SPManatomyToolbox/SPManatomyToolbox_node.html
MMP	38	Original article on multi-modal approach.	Glasser, M. F. et al. A multi-modal parcellation of human cerebral cortex. <i>Nature</i> 536, 171–178 (2016).
	39	Information on surface vs volume based methodologies for localization of neuroanatomy.	Coalsion, T. S., Van Essen, D. C. & Glasser, M. F. The impact of traditional neuroimaging methods on the spatial localization of cortical areas. <i>Proc Natl Acad Sci USA</i> 115, E6356–E6365 (2018).
	40	Website to download data. Volumetric version also included in DSi-studio. Note the volume note above.	https://balsa.wustl.edu/

Table S1. (cont.) Atlas sources and references. | This table provides a short note and references to the source material of common atlases in the neuroscience literature. See also [Table 1](#).

Please see the end of this document for a high-resolution, highlightable version

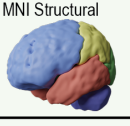
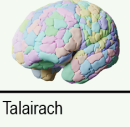
Atlas	Source	Note	Reference(s)
	41	Random atlas algorithm (pseudo-grassfire algorithm).	Zalesky, A. et al. Whole-brain anatomical networks: does the choice of nodes matter? <i>NeuroImage</i> 50, 970–83 (2010).
	42	Use case of random atlas. Goni et al. (2014) study the structure-function relationship in the brain with tractography and fMRI. They used random cortical atlases of 1170 equally sized regions. Misić et al. (2015) used random cortical atlases of 1015 equally sized regions.	(1) Goni, J. et al. Resting-brain functional connectivity predicted by analytic measures of network communication. <i>Proceedings of the National Academy of Sciences</i> 111, 833–838 (2014). (2) Mišić, B. et al. Cooperative and Competitive Spreading Dynamics on the Human Connectome. <i>Neuron</i> 86, 1518–29 (2015).
	43	Included with FSL. See website for further details. Included structures are (1) Caudate, (2) Putamen, (3) Thalamus, (4) Insula, (5) Frontal lobe, (6) Temporal lobe, (7) Parietal lobe, (8) Occipital lobe, and (9) Cerebellum.	(1) Website: http://www.talairach.org/about.html (2) http://www.talairach.org/about.html (3) Maziotta, J. et al. A probabilistic atlas and reference system for the human brain: International Consortium for Brain Mapping (ICBM). <i>Phil. Trans. R. Soc. Lond. B</i> 356, 1293–1322 (2001).
	44	Original publication about functional parcellations.	Schaefer, A. et al. Local-Global Parcellation of the Human Cerebral Cortex from Intrinsic Functional Connectivity MRI. <i>Cerebral Cortex</i> 28, 3095–3114 (2018).
	45	GitHub and detailed documentation of atlases.	https://github.com/ThomasYeoLab/CBIG/tree/master/stable_projects/brain_parcellation/Schaefer2018_LocalGlobal
	46	Download: Included with FSL. Also available through website.	Website: http://www.talairach.org/
	47	The anatomical region labels were electronically derived from axial sectional images in the 1988 Talairach Atlas. The atlas was digitized and manually traced into a volume-occupant hierarchy of anatomical regions detailed these publications (i.e. the pages of the 1988 textbook with drawings were photocopied and transformed into the computerized coordinate system).	(1) Lancaster, J. L., Evans, A. C. & Toga, A. W. Automated Labeling of the Human Brain: A Preliminary Report on the Development and Evaluation of a Forward-Transform Method. 238–242 (1997). (2) Lancaster, J. L. et al. Automated Talairach Atlas Labels For Functional Brain Mapping. 120–131 (2000).
	48	(1) First atlas in 1957 focusing on the subcortical deep gray nuclei, (2) second atlas in 1967 focusing on the telencephalon, (3) third atlas in 1988 focusing on the whole brain. Most researchers preferred the use of the Talairach atlas to report the localization of the activations detected in functional imaging studies because it offers a detailed anatomical brain description within the stereotaxic space, including Brodmann's areas.	(1) Talairach, J., David, M., Tournoux, P., Corredor, H. & Kvasina, T. <i>Atlas d'Anatomie Stéréotaxique. Repérage Radiologique Indirect des Noyaux Gris Centraux des Régions Mésencephalosousoptique et Hypothalamique de l'Homme.</i> (1957). (2) Talairach, J. & Szikla, G. <i>Atlas of Stereotaxic Anatomy of the Telencephalon.</i> (Masson, 1967) (3) Talairach, J. & Tournoux, P. <i>Co-planar stereotaxic atlas of the human brain: 3-dimensional proportional system: an approach to cerebral imaging.</i> (Georg Thieme, 1988).
	49	Historical publication about Jean Talairach.	Harary, M. & Cosgrove, G. R. Jean Talairach: a cerebral cartographer. <i>Neurosurgical Focus</i> 47, E12 (2019).
	50	Comparison between MNI and Talairach Coordinates.	Lancaster, J. L. et al. Bias between MNI and Talairach coordinates analyzed using the ICBM-152 brain template. <i>Hum. Brain Mapp.</i> 28, 1194–1205 (2007).
	51	Original publication about functional parcellations.	Thomas Yeo, B. T. et al. The organization of the human cerebral cortex estimated by intrinsic functional connectivity. <i>Journal of Neurophysiology</i> 106, 1125–1165 (2011)
	52	Website from FreeSurfer.	https://surfer.nmr.mgh.harvard.edu/fswiki/CorticalParcellation_Yeo2011
	53	Thalamus - based on ex vivo analysis.	Iglesias, J. E. et al. A probabilistic atlas of the human thalamic nuclei combining ex vivo MRI and histology. <i>NeuroImage</i> 183, 314–326 (2018).
	54	Hippocampus - based on ex vivo analysis.	Iglesias, J. E. et al. A computational atlas of the hippocampal formation using ex vivo, ultra-high resolution MRI: Application to adaptive segmentation of in vivo MRI. <i>NeuroImage</i> 115, 117–137 (2015).
	55	Structural atlas of Cerebellum. Included with FSL.	Diedrichsen, J., Balsters, J. H., Flavell, J., Cussans, E. & Ramnani, N. A probabilistic MR atlas of the human cerebellum. <i>NeuroImage</i> 46, 39–46 (2009).
	56	Functional atlas of Cerebellum.	(1) Xue, A. et al. The Detailed Organization of the Human Cerebellum Estimated by Intrinsic Functional Connectivity Within the Individual. 69. (2) Buckner, R. L., Krienen, F. M., Castellanos, A., Diaz, J. C. & Yeo, B. T. T. The organization of the human cerebellum estimated by intrinsic functional connectivity. <i>Journal of Neurophysiology</i> 106, 2322–2345 (2011). (2) GitHub: https://github.com/ThomasYeoLab/CBIG/tree/master/stable_projects/brain_parcellation/Xue2021_IndCerebellum
	57	Pediatric/Neonatal.	Alexander, B. et al. A new neonatal cortical and subcortical brain atlas: the Melbourne Children's Regional Infant Brain (M-CRIB) atlas. <i>NeuroImage</i> 147, 841–851 (2017).
	58	Disease-specific: example of a multiple sclerosis lesional atlas.	Sahraian, M. A. & Radue, E.-W. <i>MRI atlas of MS lesions.</i> (Springer, 2008).

Table S1. (cont.) Atlas sources and references. | This table provides a short note and references to the source material of common atlases in the neuroscience literature. See also [Table 1](#).

Atlas Morphology: Sizes and Shapes

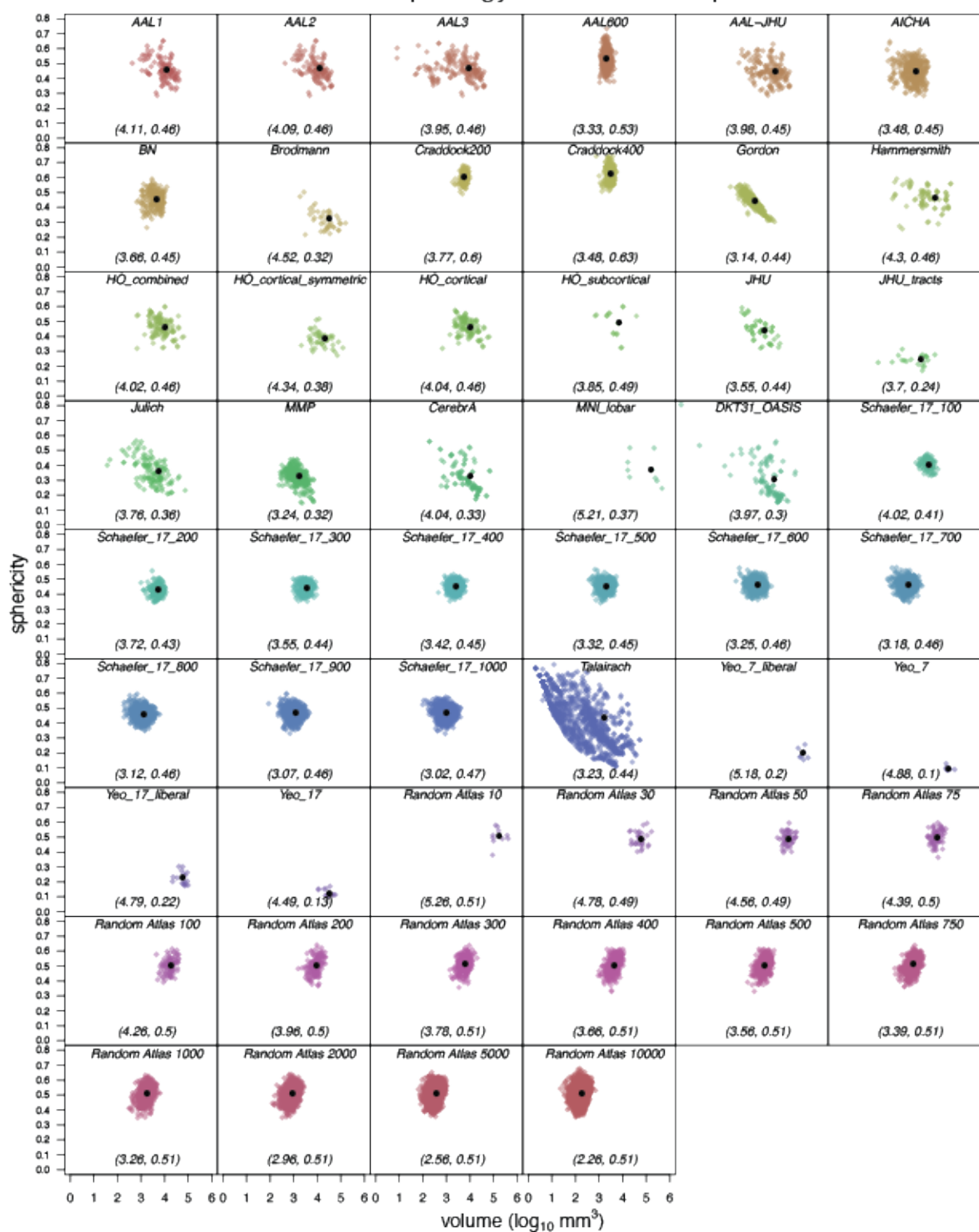


Fig. S2. Atlas Morphology: Sizes and Shapes. | All standard atlases and one permutation for each of the standard atlases are shown here. Volume means and sphericity means are in parentheses at the bottom of each graph. See [Table S1](#) for atlas abbreviations, descriptions, and sources.

Remaining atlases (Repeat of Fig. 3)

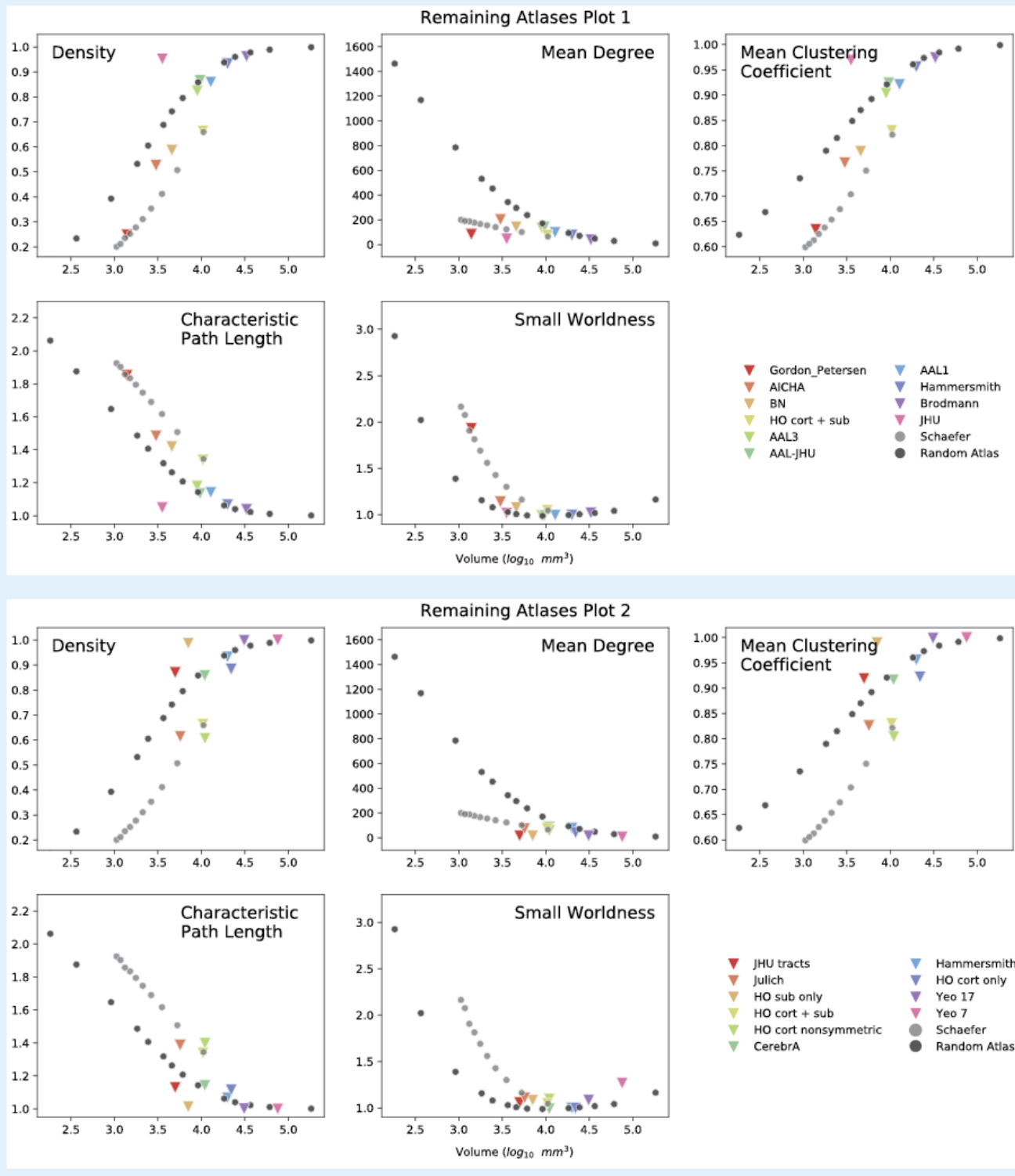


Fig. S3. Structure-Function Correlation (SFC) for All Atlases. | We show network measures the remaining atlases illustrated in Table 2. See Table S1 for atlas descriptions. **HO**, Harvard-Oxford; **Sub**, subcortical; **Cort**, cortical

Controls and patients separated (Repeat of Fig. 3)

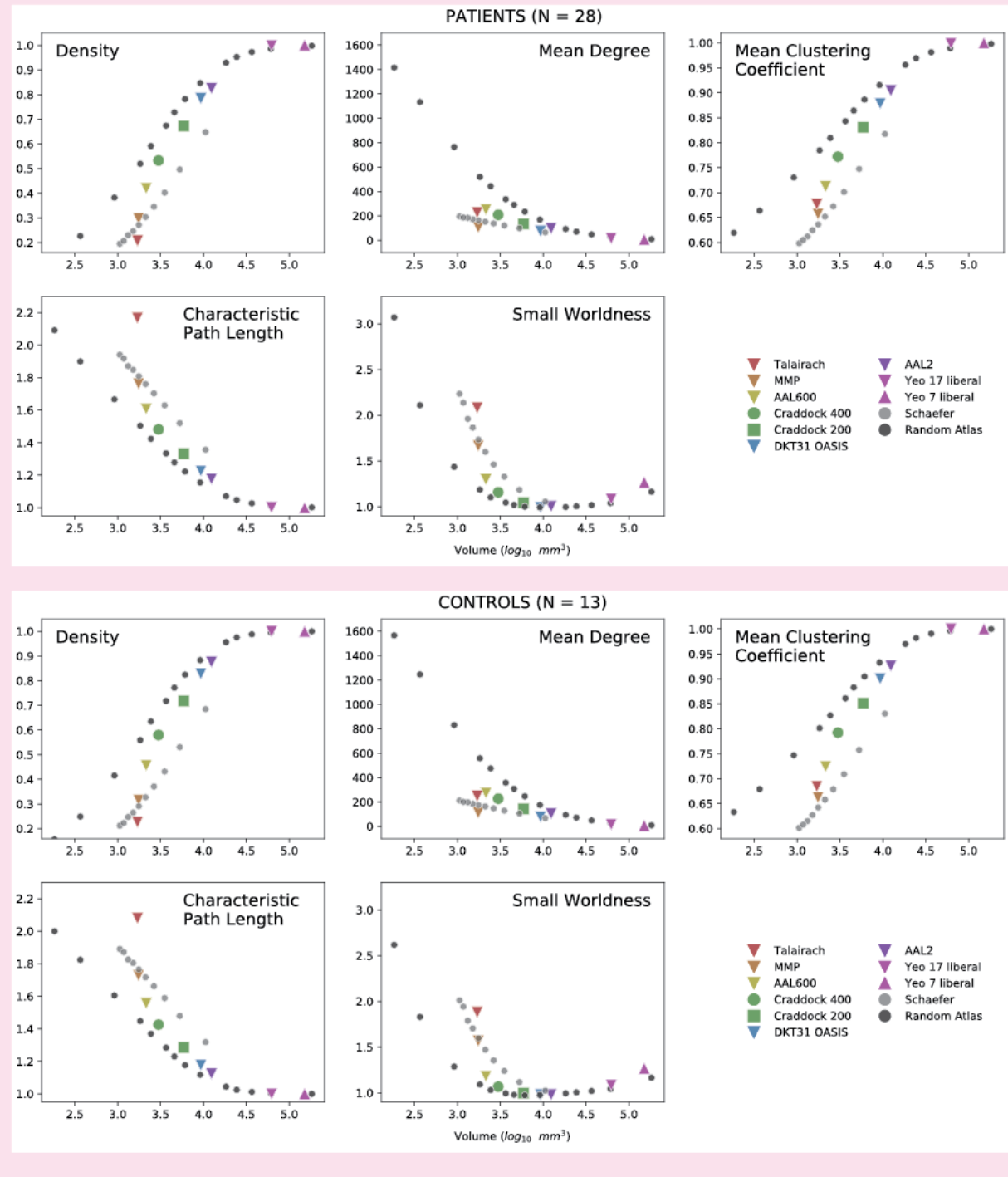


Fig. S4. Network Measures: Controls vs Patients. | We replicate Fig. 2 (N=41) in the manuscript by separating out controls (N=13) and patients (N=28). All global network measures above are similar between patients and controls, with patients having slightly lower (but not significant, Fig. 2 bottom right panel) measurements for the different network properties. Specific connectivity differences between controls and patients were not explored (e.g. to explore if connections from the hippocampus to the anterior cingulate are changed in temporal lobe epilepsy) and out of the scope of this manuscript. See Table S1 for atlas descriptions.

Re-calculating network measures at different thresholds (Repeat of Fig. 3)

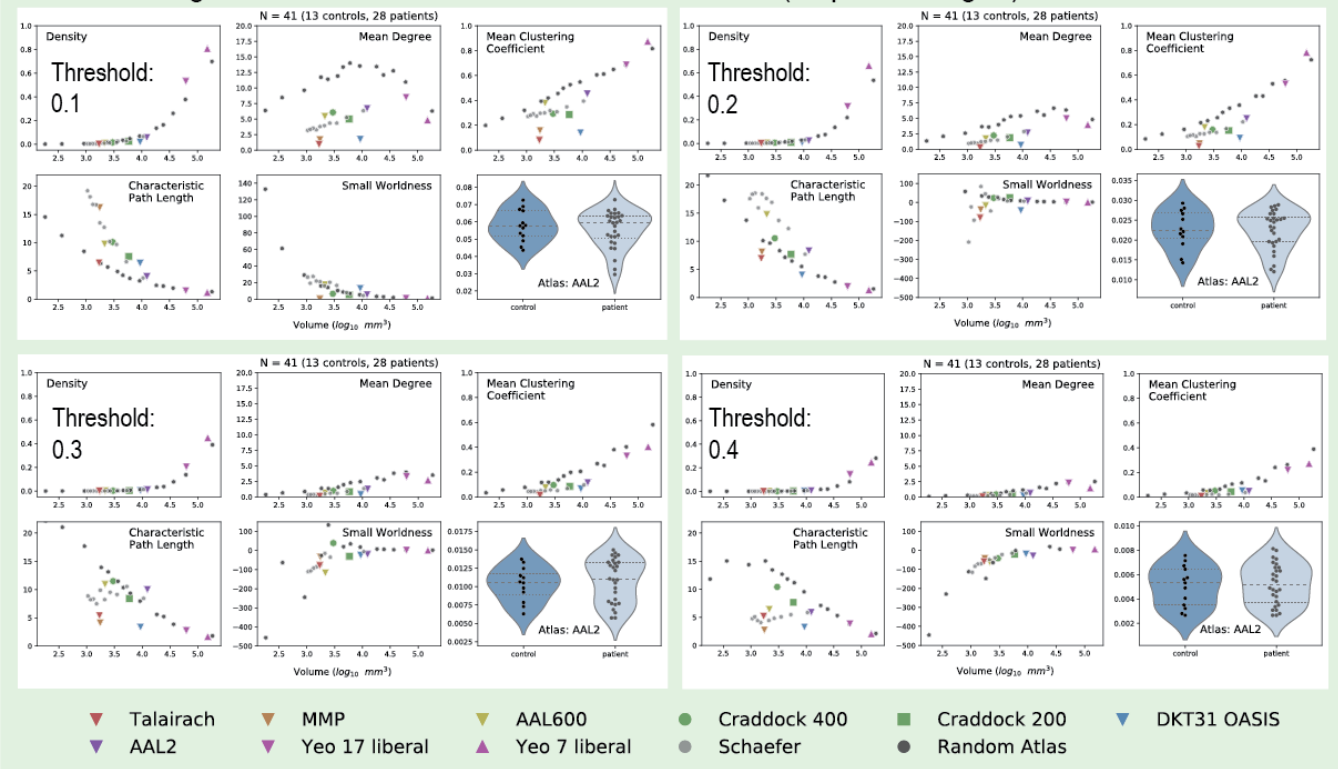


Fig. S5. Network Measures: different thresholds. | We replicate Fig. 2 (N=41) in the manuscript by calculating network measures using different thresholds. The main text figure includes all weights with no threshold (threshold = 0). We set thresholds at 01., 0.2, 0.3, and 0.4. This was done to show how various network measures may also change when eliminating low-level connections at different thresholds.

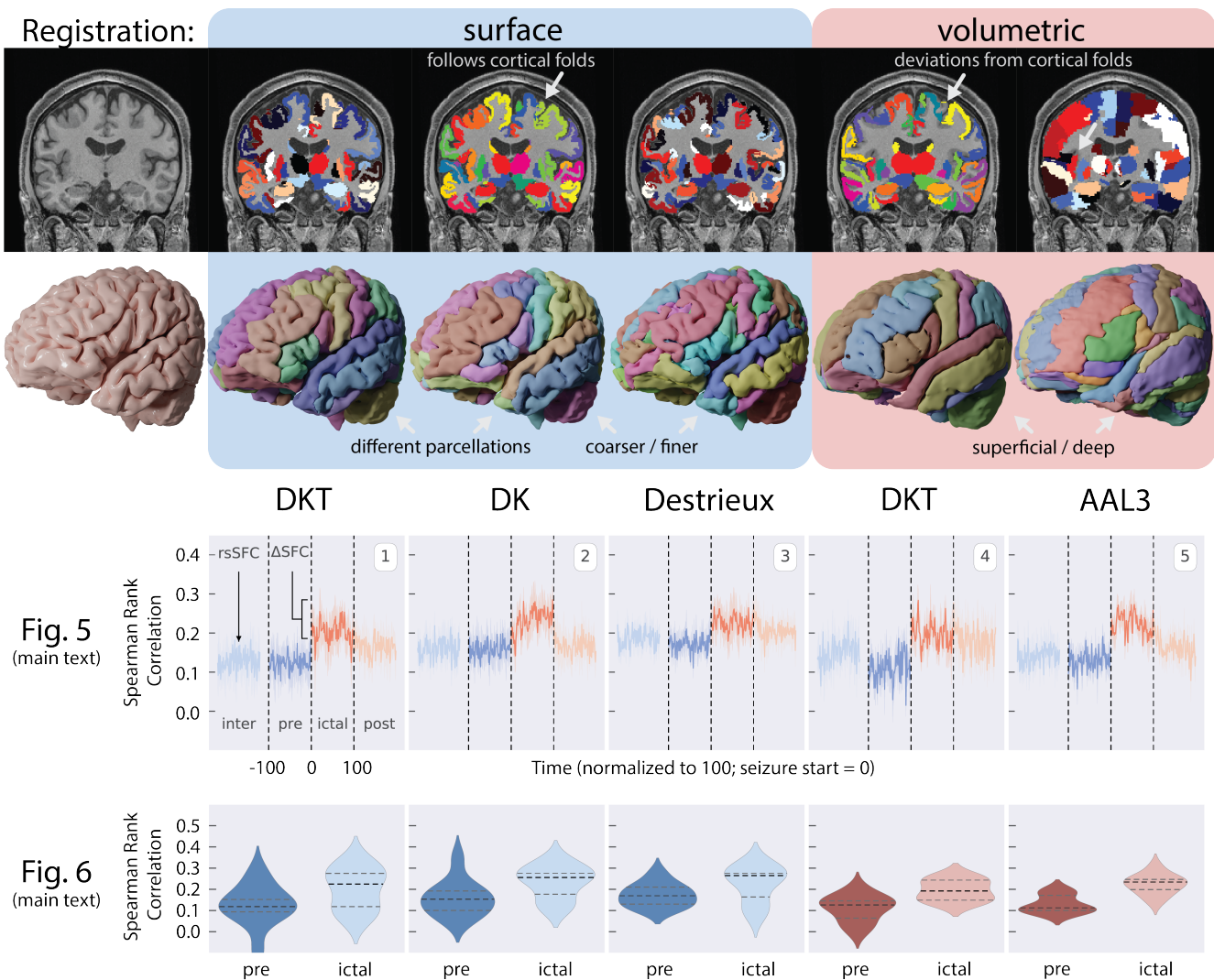


Fig. S6. Effects of Registration: Volumetric- and Surface-based approaches | Volumetric-based analyses, as opposed to surface-based analyses, have been more prevalent in human neuroimaging studies for the last few decades²¹. Volumetric-based approaches to map the neocortex have been shown to be inaccurate in some cases. For example, the top row shows a single subject's T1w image and the resulting labels of three atlases registered using a surface-based approach and two atlases using a volumetric-based approach. The DKT atlas using a surface-based approach follows the cortical folds of the T1w image closely, but the DKT atlas registered using a volumetric-based approach may have many mis-aligned areas. These images show the improved accuracy in mapping and labeling brain structures using surface-based analyses, but the adoption of surface-based analyses has been slow and attributed to five main reasons discussed in Coalson et. al 2018²¹. Briefly, it is due to (1) the need to compare results with existing volumetric-based studies, (2) the prevalence of volumetric-based tools compared to surface-based tools, (3) the learning curve of surface-based approaches; (4) an unawareness of the problems and benefits of each approach; (5) and uncertainty or skepticism as to how much of a difference these methodological choices make. In some cases, it may make a difference, however, it does not make a difference in this study. Here, we used a surface-based approach to register three different atlases to each patient. The atlases were outputs of FreeSurfer's recon-all pipeline⁷⁸ - the DKT40, Desikan-Killiany (DK), and Destrieux atlases. The DKT atlas has a modified parcellations of the DK atlas, and the Destrieux atlas is an alternative atlas offered by the FreeSurfer pipeline. The Destrieux atlas has a finer parcellation scheme (i.e., more number of regions). We repeat analyses of Fig. 5 and Fig. 6 of the main text, along with results from two volumetric-based atlases for side-by-side comparison. The volumetric-based atlases include the DKT (DKT31 OASIS) and AAL3 atlases. While the volumetric DKT atlas does not properly align and label the entire cortical gray matter regions, the AAL atlas extends deeply into the white matter and does label much of these gray matter regions. For the experimental design of this study in localizing electrode contacts and measuring structural connectivity, the AAL3 atlas provides the most power out of all these atlases in detecting a change in SFC. In the original AAL manuscript⁸⁸, the authors "chose to extend the internal limit of the regions beyond the gray matter layer [to account for] anatomical variability". This extension past the internal gray matter boundary may be optimal in our case for measuring SFC because the parcellations may capture streamlines that otherwise would have ended prematurely before reaching gray matter.

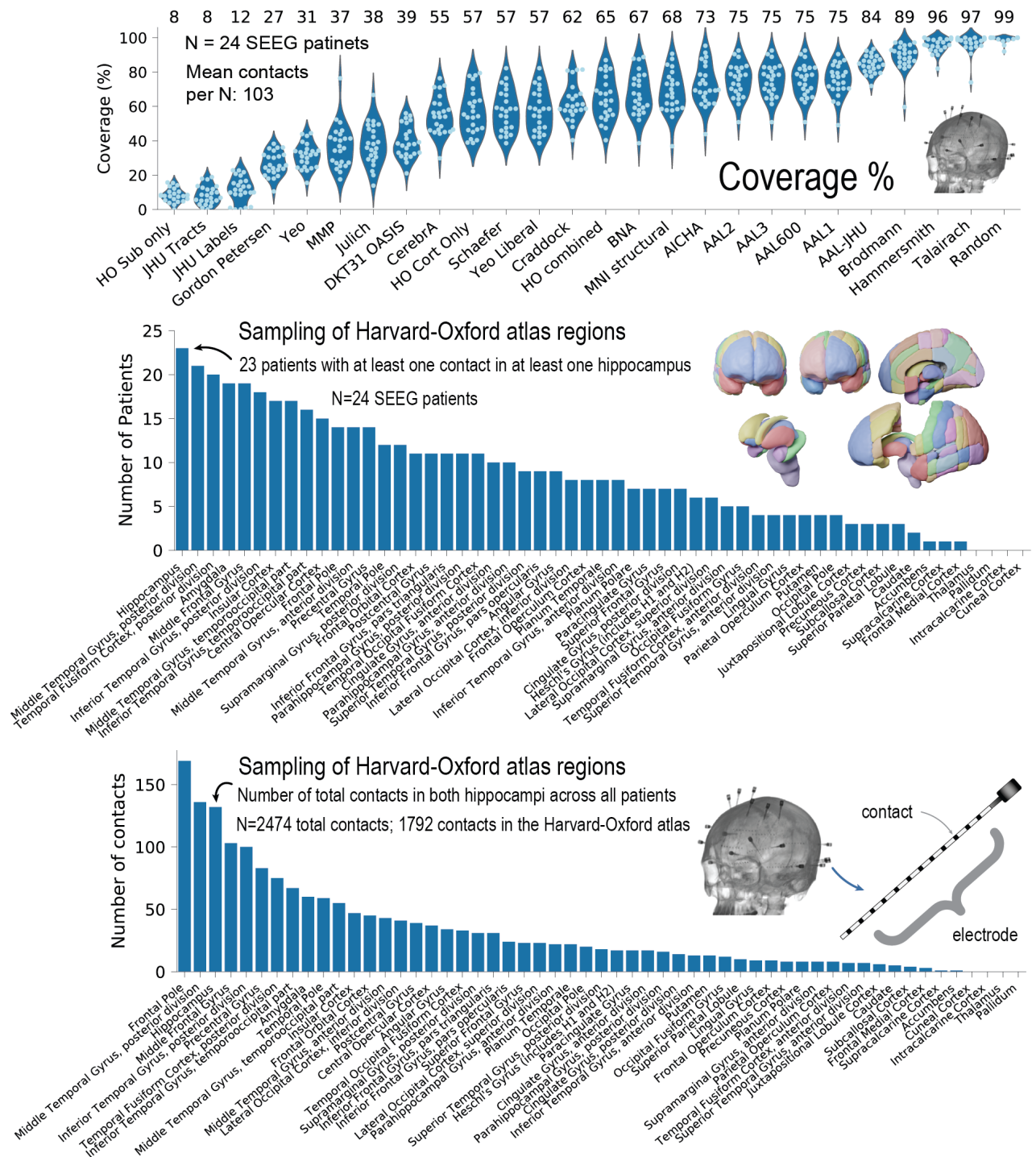


Fig. S7. Coverage of electrode contacts. | Top: We show the percentage of contacts assigned a region given an atlas. If a contact fell outside an atlas, it would not be assigned a location and would not be used in SFC analysis. We also show the Harvard-Oxford atlas regions (cortical and subcortical combined) that contain electrode contacts (middle and bottom figures). The middle figure shows the number of patients with at least one contact in an atlas region (at least one of the regions on both hemispheres). The bottom figure shows the total number of contacts in each listed region. Note that 1792 out of 2474 contacts (72%) contained within the brain parenchyma (gray matter or white matter) is higher than the mean percent coverage listed in the top figure (65% for the HO combined) because some patients with fewer contacts may have lower coverage by the atlas, thus bringing the mean percent down. Also note the larger number of contacts in the frontal pole because this region in the Harvard-Oxford atlas is large. We chose to show the Harvard-Oxford atlas because it has the largest effect size in Fig. 6.

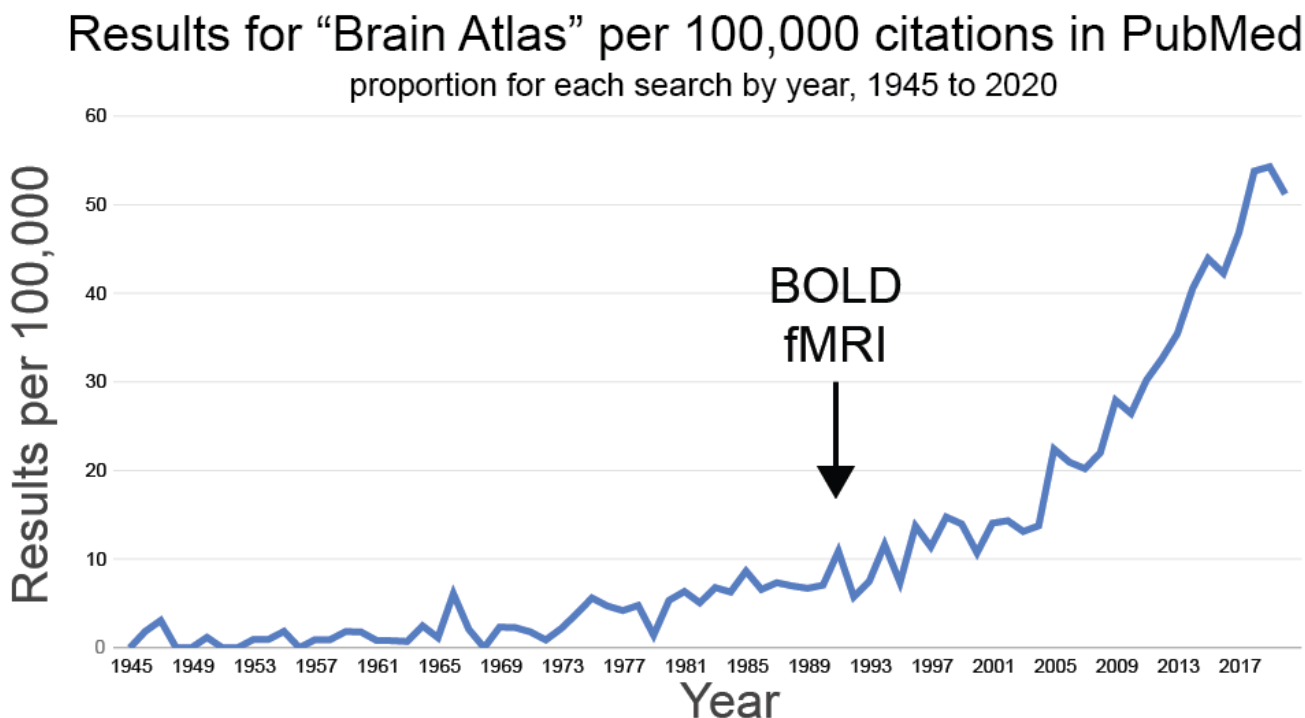


Fig. S8. The increase in publications related to brain atlases. | We searched for any publications since 1945 using the term “Brain Atlas” on PubMed. We note that since the introduction of BOLD fMRI in 1990, the need for neuroanatomical maps of the brain has increased, especially in the neuroimaging community. Many atlases have been published over the last 30 years, and many publications across the neuroscience literature have used these atlases. However, no comprehensive study exists evaluating, in any regard, to the suitability and nuances related to these atlases. We hope our work provides a valuable resource to others in our field, launches a larger discussion to critically evaluating the neuroanatomy of the brain, and direct future reproducible research for other scientists and clinician investigators.

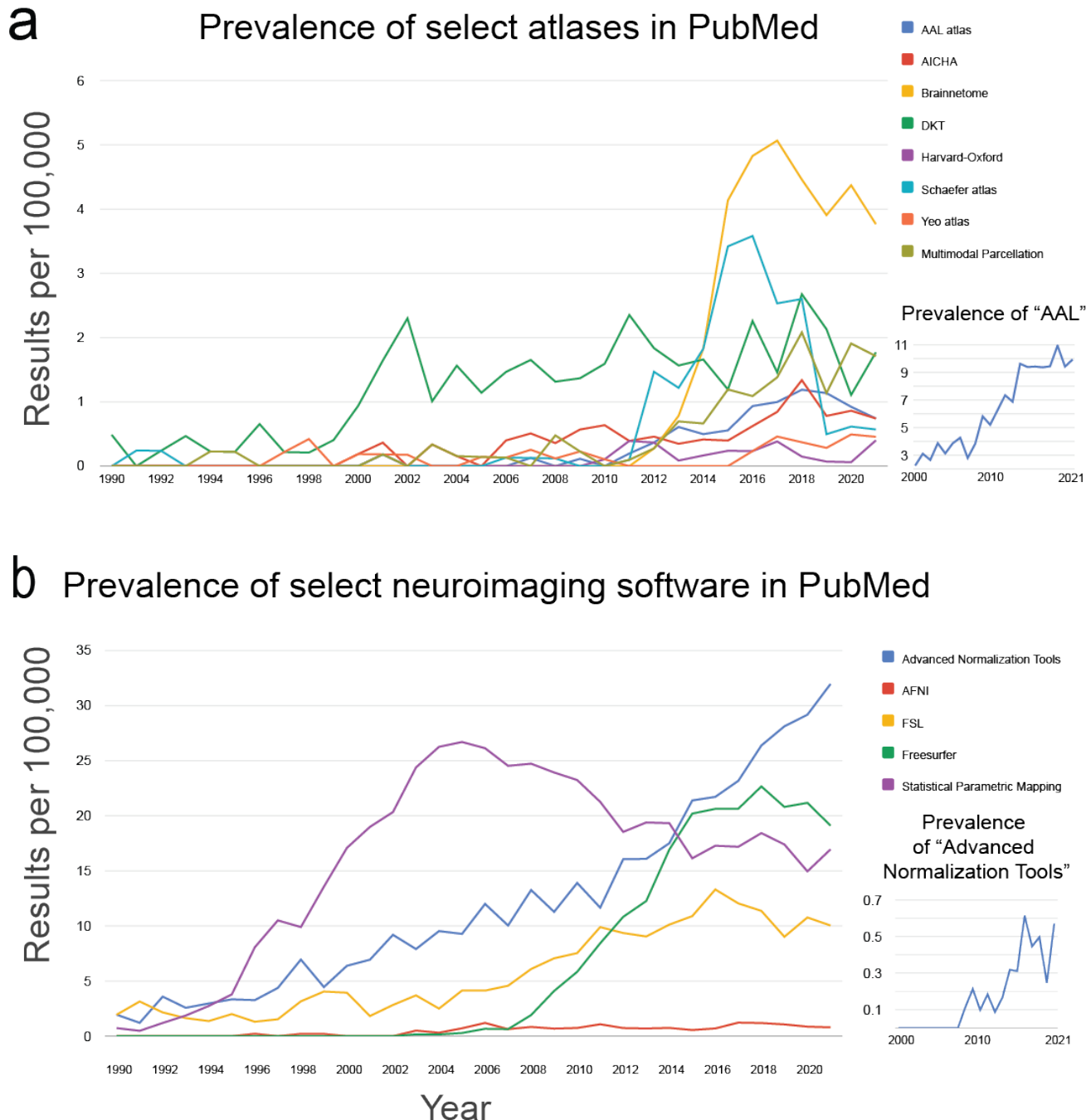


Fig. S9. Prevalence of select brain atlases and neuroimaging software | a, We searched on PubMed for any publications since 1945 using the verbatim terms shown in each line graph legend. The tool used is from <https://esperr.github.io/pubmed-by-year/>⁸⁹. This search was done to gain a better understanding how often the field is using different tools, and thus to make some recommendations as to which atlases to use and facilitating the comparison of results. Note that due to the prevalence of the term "AAL" which may not relate to the AAL atlas, we opted for the term "AAL atlas". Another example is the use of "Multimodal Parcellation" rather than "MMP". The search for "AAL" is shown at the bottom right, where articles appear before the original AAL manuscript in 2002⁸⁸, most likely not relating to the AAL atlas. However, the prevalence of "AAL" increases substantially after 2002, more than other atlases. These search terms serves as a rough estimate of the prevalence of atlases, and may not reflect the true prevalence of each term. **b**, We show to prevalence of select neuroimaging software. Again, due to the ambiguity of search terms such as "ANTS", we opted for the full name of the software, despite some manuscripts only having used the abbreviated terms. "Advanced normalization tools" searched in quotes is shown at the bottom right, having first appeared formally in the literature in 2009⁹⁰.

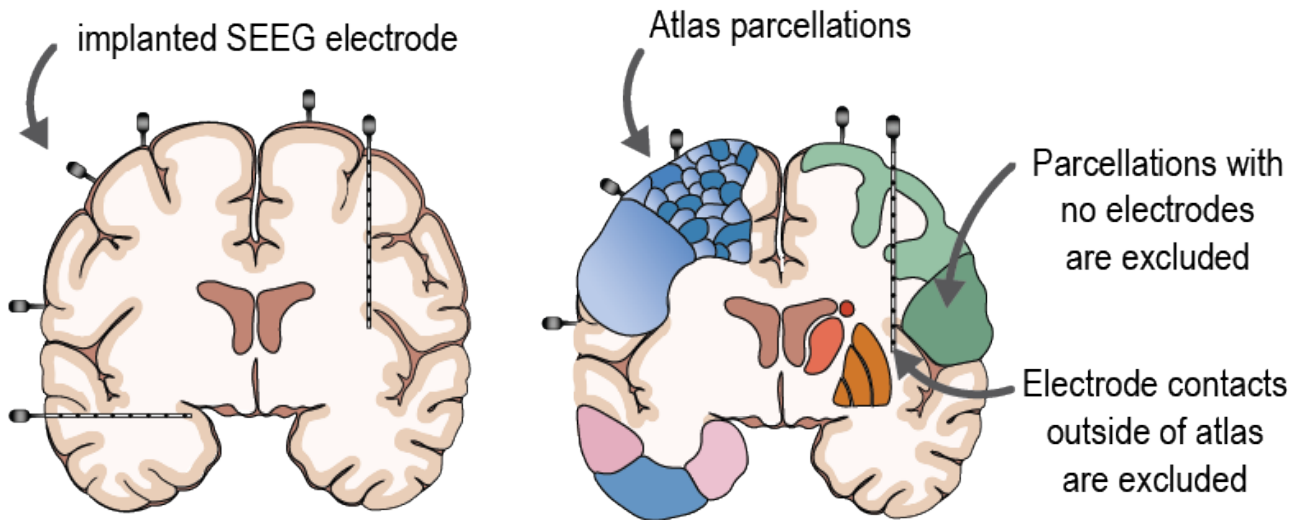


Fig. S10. Electrode localization and region selection | Assignment of each electrode contact to an atlas regions was performed by rounding electrode coordinates (x,y,z) to the nearest voxel and indexing the given atlas at that voxel. Electrodes that fell outside the atlas of interest were excluded from subsequent analysis. The structural connectivity network, representing normalized streamline counts between each atlas region, was also down sampled to only include regions that contained at least one SEEG contact. This gave one static representation of structural connectivity. In the case where multiple electrodes fell in the same atlas ROI, a random electrode was selected to represent the functional activity of that neuroanatomically defined region.

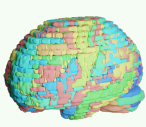
Patient	Age	Sex	Localization: suspected seizure onset zone	Control	Age	Sex
sub-patient01	58	M	Poorly localized. R temporal interictal activity.	sub-control01	24	M
sub-patient02	28	F	L anterior temporal lobe	sub-control02	40	F
sub-patient03	27	F	L hippocampus and amygdala	sub-control03	31	M
sub-patient04	20	F	L basal ganglia infarct	sub-control04	29	M
sub-patient05**	36	M	R frontal arteriovenous malformation	sub-control05	40	M
sub-patient06	57	F	Poorly localized. Possibly bitemporal onset	sub-control06	48	F
sub-patient07**	37	M	L temporal lobe/hippocampus/amygdala	sub-control07	22	M
sub-patient08**	34	M	R frontal, anterior cingulate gyrus	sub-control08	35	F
sub-patient09**	47	F	L hippocampus	sub-control09	27	F
sub-patient10	42	F	R temporal lobe/L temporal lobe	sub-control10	67	F
sub-patient11	27	M	L hippocampus, then amygdala	sub-control11	33	F
sub-patient12	35	M	Poorly localized. Possibly multifocal epilepsy	sub-control12	27	M
sub-patient13**	36	F	L temporal	sub-control13	NR	NR
sub-patient14**	29	F	L superior Frontal Sulcus			
sub-patient15	33	F	L mesial temporal lobe			
sub-patient16	29	M	Poorly localized. Possibly multifocal epilepsy			
sub-patient17	31	F	L mesial temporal lobe			
sub-patient18**	26	F	L heterotopia, left hippocampus			
sub-patient19**	23	M	L temporal/posterior lateral neocortical			
sub-patient20	30	M	L temporal encephalomalacia			
sub-patient21	24	M	R anterior temporal lobe			
sub-patient22	59	F	R frontal-parietal lobe			
sub-patient23	28	F	L or R superior temporal gyrus			
sub-patient24**	47	F	R anterior temporal			
sub-patient25	40	F	L temporal lobe near Heschl's gyrus			
sub-patient26	37	F	L amygdala/anterior temporal pole			
sub-patient27	30	M	L amygdala/hippocampus			
sub-patient28**	28	M	L mesial temporal lobe			

Table S2. Patient and control demographics. Patient IDs with asterisk have clinically annotated seizures for structure-function calculation. Localization of the seizure onset zone was pulled from patient charts, either from the clinically hypothesized brain regions if the patient did not undergo surgery, or if the patient underwent surgery, the targeted location for resection or ablation. One control did not have age or sex information. **M**, Male; **F**: Female; **L**, left; **R**, Right; **NR**, Not reported

Atlas [regions]	Sources	3D Render	Description	Variations
AAL [116;120;166]	1-7 SPM	S	Structural atlas. Manual identification using a defined labeling protocol on single subject template (Collin-27). Three versions. Version 2: updated boundaries. Version 3: further parcellations. Successor to Talairach.	AAL: AAL1, AAL2, AAL3, AAL600, AAL-JHU AAL1 AAL2 AAL3 AAL600 AAL-JHU (JHU labels blue) Removed (dark blue) Smaller (light blue) Added (red-yellow)
AICHA [384]	8	F	Functional atlas based on rsfMRI; 281 subjects. Each ROI has (1) homogeneity in its functional activity (2) a homotopic contralateral counterpart with which it has maximal connectivity.	
Brainnetome [246]	9-10 DSstudio	S	Connectivity-based parcellation. Based on idea that clustered regions of a brain region should share similar connectivity profiles; 40 subjects from HCP dataset. 210 cortical; 36 subcortical.	
Brodmann [48]	11-13 MRIcron	S	Developed by independent group at Washington University in St. Louis. Published with MRIcron software. Warned by developer to be used with caution - not validated, nor based on multiple individuals.	
CerebrA [102]	14	S	Structural atlas. Non-linear registration of cortical and subcortical labelling from Mindboggle-101 dataset (see DKT below) to the symmetric MNI-ICBM2009c template, followed by manual editing.	Craddock: N parcellations N=200 N=400 1.7 cm 1.0 cm pea
Craddock [N]	15-17	F	Functional atlas; rsfMRI; 41 subjects. ROIs are spatially clustered into regions of homogeneous functional connectivity. May be N regions. 200/400 regions publicly available. 4x4x4 mm ³ resolution fMRI. Resliced.	
DKT [109]	18-23 FreeSurfer	S	DKT is a labelling protocol. DK is old protocol. Used on Mindboggle-101 dataset (101 brains). Probabilistic atlas using joint fusion algorithm. Surface version in FreeSurfer (40 brains). Volumetric version, 20 brain subset. Non-cortical: Neuromorphometrics BrainCOLOR atlas (aseg).	DKT: Surface (probabilistic labeling of individual with surface-based registration), Volumetric (labeling with volumetric-registration) DKT surface DK surface DKT volumetric
Destrieux [189]	24-25 FreeSurfer	S	Probabilistic atlas of surface anatomy created from: (1) Manual labeling, (2) surface geometry, (3) spatial relationship of neighboring structures. Available in FreeSurfer with subcortical structures added.	Harvard-Oxford: Cortical/subcortical only, combined, symmetric, nonsymmetric Symmetric Nonsymmetric Subcortical Combined Cortical + Subcortical
Gordon-Petersen [333]	26-27	F	Identification of abrupt transitions in resting-state functional connectivity to identify parcellations. Based on rsfMRI. 108 subjects. Intended for surface-based analyses.	
Hammersmith [83]	28-30	S	Manually identified 83 structures using defined labelling protocol; 30 subjects. Maximum probability map. First version in 2003 with 49 structures. Named after London hospital, Hammersmith. Hammers is author.	
Harvard-Oxford [48 + 21]	31-32 FSL	S	Manual segmentation using defined labelling protocol; 37 subjects. Cortical and subcortical atlases provided separately. Left and right structures have same labels (symmetry). Must preprocess.	
JHU [48; 20]	33-35 FSL	S	White matter atlas. Two versions. (1) Labels: Hand segmentation average of diffusion MRI; 81 subjects. (2) Tracts: probabilistic identification from deterministic tractography; 28 subjects.	JHU: Labels, tracts Labels Tracts
Julich [121]	36-37 FSL	S	Cytoarchitecture atlas. Successor to Brodmann. Average of 10-subject post-mortem cyto- and myelo-architectonic segmentations. Update to the Eickhoff SPM Anatomy Toolbox v1.5. Whole brain is not covered.	
MMP [380]	38-40 DSstudio	M	Multi-modal parcellation: (1) Architecture - T1w/T2w myelin maps + cortical thickness, (2) function - task-fMRI, (3) connectivity, (4) topography. 210 subjects. Cortical ONLY. Originally intended for surface analysis. Volumetric version independently created and used.	Random: N parcellations, cortical, whole-brain, subparcellated N=30 N=10 N=100 N=1,000 N=10,000 lemon 5 cm grape 2 cm pea 1 cm
Random [N]	41-42	V	Brain is randomly parcellated into N regions. Variations used in studies include cortical and whole-brain. Other atlases (e.g. AAL) and their regions may be further randomly divided, or subparcellated.	
MNI Structural [9]	43 FSL	S	9 regions, including lobar and some subcortical regions. Hand segmented 50 subjects. Transformed into MNI152 space, averaged, probability maps produced. 25% max probability is shown.	Schaefer: 100 to 1,000 parcellations (by 100), named to Yeo 7 and 17 N=100 N=500 N=1,000
Schaefer [100-1000]	44-45 GitHub	F	Based on rsfMRI. Clusters found with gradient-weighted Markov Random Field model. 1489 subjects. Cortical only. Spatial resolutions provided: 100 - 1000 parcellations (by 100). Well documented.	
Talairach [1105]	46-50 FSL	S	Conversion of original Talairach labeling. Digitized version of the original (coarsely sliced) Talairach atlas and registration to MNI 152 space. Atlas provided in FSL.	Yeo: 7/17 parcellations; Cortically bounded or liberal Cortically bounded liberal discontinuous
Yeo [7; 17]	51-52 FreeSurfer	F	1000 subjects; rsfMRI. Clustered cortical regions by pattern of functional connectivity. Results in non-spatially continuous clusters. 7 and 17 clusters based on stability of clustering algorithm.	
Region-specific	53-56 FSL	V	Atlases created for specific regions, usually high quality + high degree of accuracy (e.g. post-mortem histological verification). Examples: Thalamus nuclei, hippocampus, and other specific structures.	Thalamus, Hippocampus, Cerebellum Cerebellum
Population-specific	57-58	V	Atlases created from a specific population (e.g. elderly, pediatric, non-human). Disease-specific defines regions specific for disease (e.g. MS lesion probabilistic locations).	Pediatric, Elderly, Disease specific Neonatal M-CRIB (Melbourne)

Atlas	Source	Note	Reference(s)
AAL	1	AAL1. The successor to the Talairach atlas. The goal was to reduce confusion in relating stereotaxic space (a set of brain coordinates) and anatomical labels. It is based on a single individual (the Collin-27 template) and it is not a probabilistic map. The Collin-27 template was intended for segmentation, and not stereotaxy; it did not capture anatomical variability. However, the high resolution in 1998 proved attractive to research groups.	(1) Tzourio-Mazoyer, N. et al. Automated Anatomical Labeling of Activations in SPM Using a Macroscopic Anatomical Parcellation of the MNI MRI Single-Subject Brain. <i>NeuroImage</i> 15, 273–289 (2002). (2) Collin-27 template: Holmes, C. J. et al. Enhancement of MR Images Using Registration for Signal Averaging: <i>Journal of Computer Assisted Tomography</i> 22, 324–333 (1998). (3) Website about Collin-27: https://www.bic.mni.mcgill.ca/ServicesAtlases/Colin27
	2	AAL2: new parcellation of orbitofrontal cortex. AAL1 orbitofrontal cortex was parcellated according to a French publication by Jules Déjerine in 1895. Chiavaras and Petrides (2000) proposed another parcellation of the orbital surface allowing for the comparison of human frontal lobe anatomy with that of macaques.	(1) Rolls, E. T., Joliot, M. & Tzourio-Mazoyer, N. Implementation of a new parcellation of the orbitofrontal cortex in the automated anatomical labeling atlas. <i>NeuroImage</i> 122, 1–5 (2015). (2) Chiavaras, M. M. & Petrides, M. Orbitofrontal sulci of the human and macaque monkey brain. <i>The Journal of Comparative Neurology</i> 422, 35–54 (3) Déjerine, J. <i>Anatomie des centres nerveux</i> . (Rueff Paris, 1895).
	3	AAL3: new parcellations - anterior cingulate, thalamus, nucleus accumbens, substantia nigra, ventral tegmental area, red nucleus, locus coeruleus, and raphe nuclei. 2019. AAL3v1: changes of thalamus in line with FreeSurfer 7. 2020.	Rolls, E. T., Huang, C.-C., Lin, C.-P., Feng, J. & Joliot, M. Automated anatomical labelling atlas 3. <i>NeuroImage</i> 206, 116189 (2020).
	4	Website for download - group that made AAL toolbox and user guides.	https://www.gin.cnrs.fr/en/tools/aal/
	5	SPM - software compatible with AAL toolbox. Generally, designed for the analysis of brain imaging data sequences. Extensions include AAL toolbox.	(1) Statistical parametric mapping: the analysis of functional brain images. (Elsevier/Academic Press, 2007). (2) Website: https://www.fil.ion.ucl.ac.uk/spm/ext/
	6	AAL 600 - Subparcellations of the AAL atlas into 600 subregions. Upsampling algorithm described. Part of larger framework for evaluating the effect of parcellation scale.	Bassett, D. S., Brown, J. A., Deshpande, V., Carlson, J. M. & Grafton, S. T. Conserved and variable architecture of human white matter connectivity. <i>NeuroImage</i> 54, 1262–1279 (2011)
	7	Use cases of AAL600. Both Ashourvan et al. (2017) and Hermundstad et al. (2014) use AAL600 for generating both structural and functional connectivity networks.	(1) Ashourvan, A., Telesford, Q. K., Verstynen, T., Vettel, J. M. & Bassett, D. S. Multi-scale detection of hierarchical community architecture in structural and functional brain networks. (2017) (2) Hermundstad, A. M. et al. Structurally-Constrained Relationships between Cognitive States in the Human Brain. <i>PLoS Comput Biol</i> 10, e1003591 (2014).
AICHA	8	AICHA tries to account for <i>homotopy</i> : the concept that each region in one hemisphere has a homologue in the other.	Joliot, M. et al. AICHA: An atlas of intrinsic connectivity of homotopic areas. <i>Journal of Neuroscience Methods</i> 254, 46–59 (2015)
Brainnetome	9	Connectivity-based atlas. Further subdivision of structural parcellations using the DK (Desikan-Killiany) protocol, with adjustments.	Fan, L. et al. The Human Brainnetome Atlas: A New Brain Atlas Based on Connectional Architecture. <i>Cerebral cortex</i> (New York, N.Y. : 1991) 26, 3508–26 (2016). Website: http://atlas.brainnetome.org
	10	DSI studio created by Fang-Cheng (Frank) Yeh. Many reconstruction and tracking algorithms are published and incorporated into DSI Studio. See citations page on website. Many atlases available, including Brainnetome. Can use custom atlas.	(1) Website: http://dsi-studio.labsolver.org/ (2) Example of reconstruction method: Fang-Cheng Yeh, Wedeen, V. J. & Tseng, W.-Y. I. Generalized q-Sampling Imaging. <i>IEEE Trans. Med. Imaging</i> 29, 1626–1635 (2010).
Brodmann	11	Perspective, description, and historical significance of Korbinian Brodmann's map.	Zilles, K. & Amunts, K. Centenary of Brodmann's map — conception and fate. <i>Nat Rev Neurosci</i> 11, 139–145 (2010)
	12	References to the original German and English translation provided.	(1) Original German: <i>Vergleichende Lokalisationslehre der Grosshirnrinde in ihren Prinzipien dargestellt auf Grund des Zellenbaues</i> . (1909) (2) English translation: Brodmann, K. & Gary, L. J. Brodmann's localisation in the cerebral cortex: the principles of comparative localisation in the cerebral cortex based on cytoarchitectonics. (Springer, 2006)
	13	The atlas is available through MRICro, a legacy tool developed by Chris Rorden (University of South Carolina). The atlas is based on work from the Van Essen lab (Washington University in St. Louis) with corresponding Talairach coordinates, and transformed by Krish Singh (Cardiff University) to MNI space.	(1) Chris Rorden legacy tools webpage: https://people.cas.sc.edu/rorden/ (2) Updated webpage: https://cml.readthedocs.io/ (3) About Brodmann atlas: https://people.cas.sc.edu/rorden/mricro/lesion.html (4) BALSA: https://balsa.wustl.edu/Wz8r
CerebrA	14	Introduction to the CerebrA and MNI-ICBM2009c average brain template.	Manera, A. L., Dadar, M., Fonov, V. & Collins, D. L. CerebrA, registration and manual label correction of Mindboggle-101 atlas for MNI-ICBM152 template. <i>Sci Data</i> 7, 237 (2020). Website: https://doi.gin.g-node.org/10.12751/g-node.be5e62
Craddock	15	Original publication about functional parcellations.	Craddock, R. C., James, G. A., Holtzheimer, P. E., Hu, X. P. & Mayberg, H. S. A whole brain fMRI atlas generated via spatially constrained spectral clustering. <i>Hum. Brain Mapp.</i> 33, 1914–1928 (2012).
	16	GitHub with source code to make atlas with N clusters.	GitHub: http://ccraddock.github.io/cluster_roi/atlas.html
	17	Publicly available pre-made atlases at N=200 and N=400 from ABIDE (Autism Brain Imaging Data Exchange), co-founded by Cameron Craddock. 4x4x4mm resolution.	ABIDE: http://preprocessed-connectomes-project.org/abide/Pipelines.html

Atlas	Source	Note	Reference(s)
DKT	18	Original DKT protocol and atlas. A protocol for an atlas is a set of instructions for how the brain should be labeled. See AAL, Hammersmith, Harvard-Oxford, and JHU atlases.	Desikan, R. S. et al. An automated labeling system for subdividing the human cerebral cortex on MRI scans into gyral based regions of interest. <i>NeuroImage</i> 31, 968–980 (2006).
	19	DKT protocol, Mindboggle-101 dataset, and atlas creation.	Klein, A. & Tourville, J. 101 Labeled Brain Images and a Consistent Human Cortical Labeling Protocol. <i>Front. Neurosci.</i> 6, (2012).
	20	Summary of Mindboggle project, history, atlas development, applications, and current problems.	Klein, A. et al. Mindboggling morphometry of human brains. <i>PLoS Comput Biol</i> 13, e1005350 (2017)
	21	Websites for downloading data including the labeled brains and atlases.	Open Science Framework: https://osf.io/nhtur/ Harvard Dataverse: https://dataverse.harvard.edu/dataverse/mindboggle Labels: https://mindboggle.readthedocs.io/en/latest/labels.html GitHub: https://github.com/nipy/mindboggle
	22	Subcortical regions.	http://www.neuromorphometrics.com/
	23	FreeSurfer.	https://surfer.nmr.mgh.harvard.edu/
Destrieux	24	Original article describes automatic labeling algorithm from probabilistic information using a manually labeled training set. 74 parcellations per hemisphere (excluding subcortical structures). Available in FreeSurfer with subcortical structures output.	(1) Destrieux, C., et al., E. Automatic parcellation of human cortical gyri and sulci using standard anatomical nomenclature. <i>NeuroImage</i> 53, 1–15 (2010). (2) Fischl, B. Automatically Parcellating the Human Cerebral Cortex. <i>Cerebral Cortex</i> 14, 11–22 (2004).
	25	FreeSurfer information on atlases available.	(1) https://surfer.nmr.mgh.harvard.edu/fswiki/CorticalParcellation (2) https://surfer.nmr.mgh.harvard.edu/fswiki/DestrieuxAtlasChanges
Gordon-Petersen	26	Original article.	Gordon, E. M. et al. Generation and Evaluation of a Cortical Area Parcellation from Resting-State Correlations. <i>Cereb. Cortex</i> 26, 288–303 (2016).
	27	Resource to download atlas.	https://sites.wustl.edu/petersenschlaggarlab/resources/
Hammersmith	28	Original article (for regions 1-49), including their Hammersmith protocol (or "algorithm").	Hammers, A. et al. Three-dimensional maximum probability atlas of the human brain, with particular reference to the temporal lobe. <i>Hum. Brain Mapp.</i> 19, 224–247 (2003).
	29	Updated regions (for regions 50-83).	Gousias, I. S. et al. Automatic segmentation of brain MRIs of 2-year-olds into 83 regions of interest. <i>NeuroImage</i> 40, 672–684 (2008).
	30	Download atlas with 83 regions.	http://brain-development.org/brain-atlases/adult-brain-atlases/adult-brain-maximum-probability-map-hammersmith-atlas-n30r83-in-mni-space/
Harvard-Oxford	31	Atlas developed at the Center for Morphometric Analysis (CMA) at Massachusetts General Hospital and distributed with FSL.	https://fsl.fmrib.ox.ac.uk/fsl/fslwiki/Atlases
	32	Individual segmentations were segmented by CMA using in-house software. Probability maps were then created. Freesurfer link (right) has archived CMA's website and contains the Harvard-Oxford labeling protocols.	Freesurfer description about CMA: http://freesurfer.net/fswiki/CMA Link to website archive: https://web.archive.org/web/20180413052010/http://www.cma.mgh.harvard.edu/
JHU	33	JHU labels: Protocol to reconstruct eleven white matter tracts and their segmentation into ROI labels. Included in FSL.	Wakana, S. et al. Reproducibility of quantitative tractography methods applied to cerebral white matter. <i>NeuroImage</i> 36, 630–644 (2007).
	34	JHU Tracts: white matter parcellation atlas based on DTI probabilistic tractography of 11 major white matter tracts. Protocol defining manually identified ROIs from which the tracts were formed are described in Wakana et al. (2005). Included in FSL.	Hua, K. et al. Tract probability maps in stereotaxic spaces: Analyses of white matter anatomy and tract-specific quantification. <i>NeuroImage</i> 39, 336–347 (2008).
	35	Textbook with more information about these atlases.	MRI atlas of human white matter. (Elsevier, Acad. Press, 2011).
Julich	36	Cytoarchitecture map. Successor to both the Brodmann and Eickhoff-Zilles atlases. The Eichhoff-Zilles is an SPM toolbox (see note is source 5 about the AAL atlas) for probabilistic cytoarchitecture.	(1) Amunts, K., Mohlberg, H., Bludau, S. & Zilles, K. Julich-Brain: A 3D probabilistic atlas of the human brain's cytoarchitecture. 6 (2020). (2) Eickhoff, S. B. et al. A new SPM toolbox for combining probabilistic cytoarchitectonic maps and functional imaging data. <i>NeuroImage</i> 25, 1325–1335 (2005)
	37	Website for the Julich Atlas and SPM toolbox.	https://www.fz-juelich.de/inm/inm-1/DE/Forschung/_docs/SPMAnatomyToolbox/SPMAnatomyToolbox_node.html
MMP	38	Original article on multi-modal approach.	Glasser, M. F. et al. A multi-modal parcellation of human cerebral cortex. <i>Nature</i> 536, 171–178 (2016).
	39	Information on surface vs volume based methodologies for localization of neuroanatomy.	Coalson, T. S., Van Essen, D. C. & Glasser, M. F. The impact of traditional neuroimaging methods on the spatial localization of cortical areas. <i>Proc Natl Acad Sci USA</i> 115, E6356–E6365 (2018).
	40	Website to download data. Volumetric version also included in DSI-studio. Note the volume note above.	https://balsa.wustl.edu/

Atlas	Source	Note	Reference(s)
	41	Random atlas algorithm (pseudo-grassfire algorithm).	Zalesky, A. et al. Whole-brain anatomical networks: does the choice of nodes matter? <i>Neuroimage</i> 50, 970–83 (2010).
	42	Use case of random atlas. Goni et al. (2014) study the structure-function relationship in the brain with tractography and fMRI. They used random cortical atlases of 1170 equally sized regions. Misić et al. (2015) used random cortical atlases of 1015 equally sized regions.	(1) Goni, J. et al. Resting-brain functional connectivity predicted by analytic measures of network communication. <i>Proceedings of the National Academy of Sciences</i> 111, 833–838 (2014). (2) Mišić, B. et al. Cooperative and Competitive Spreading Dynamics on the Human Connectome. <i>Neuron</i> 86, 1518–29 (2015).
MNI Structural	43	Included with FSL. See website for further details. Included structures are (1) Caudate, (2) Putamen, (3) Thalamus, (4) Insula, (5) Frontal lobe, (6) Temporal lobe, (7) Parietal lobe, (8) Occipital lobe, and (9) Cerebellum.	(1) Website: http://www.talairach.org/about.html (2) http://www.talairach.org/about.html (3) Mazzotta, J. et al. A probabilistic atlas and reference system for the human brain: International Consortium for Brain Mapping (ICBM). <i>Phil. Trans. R. Soc. Lond. B</i> 356, 1293–1322 (2001).
	44	Original publication about functional parcellations.	Schaefer, A. et al. Local-Global Parcellation of the Human Cerebral Cortex from Intrinsic Functional Connectivity MRI. <i>Cerebral Cortex</i> 28, 3095–3114 (2018).
	45	GitHub and detailed documentation of atlases.	https://github.com/ThomasYeoLab/CBIG/tree/master/stable_projects/brain_parcellation/Schaefer2018_LocalGlobal
	46	Download: Included with FSL. Also available through website.	Website: http://www.talairach.org/
	47	The anatomical region labels were electronically derived from axial sectional images in the 1988 Talairach Atlas. The atlas was digitized and manually traced into a volume-occupant hierarchy of anatomical regions detailed these publications (i.e. the pages of the 1988 textbook with drawings were photocopied and transformed into the computerized coordinate system).	(1) Lancaster, J. L., Evans, A. C. & Toga, A. W. Automated Labeling of the Human Brain: A Preliminary Report on the Development and Evaluation of a Forward-Transform Method. 238–242 (1997). (2) Lancaster, J. L. et al. Automated Talairach Atlas Labels For Functional Brain Mapping. 120–131 (2000).
	48	(1) First atlas in 1957 focusing on the subcortical deep gray nuclei, (2) second atlas in 1967 focusing on the telencephalon, (3) third atlas in 1988 focusing on the whole brain. Most researchers preferred the use of the Talairach atlas to report the localization of the activations detected in functional imaging studies because it offers a detailed anatomical brain description within the stereotaxic space, including Brodmann's areas.	(1) Talairach, J., David, M., Tournoux, P., Corredor, H. & Kvasina, T. <i>Atlas d'Anatomie Stéréotaxique. Repérage Radiologique Indirect des Noyaux Gris Centraux des Régions Mésencéphalosousoptique et Hypothalamique de l'Homme.</i> (1957). (2) Talairach, J. & Szikla, G. <i>Atlas of Stereotaxic Anatomy of the Telencephalon.</i> (Masson, 1967) (3) Talairach, J. & Tournoux, P. Co-planar stereotaxic atlas of the human brain: 3-dimensional proportional system: an approach to cerebral imaging. (Georg Thieme, 1988).
	49	Historical publication about Jean Talairach.	Harary, M. & Cosgrove, G. R. Jean Talairach: a cerebral cartographer. <i>Neurosurgical Focus</i> 47, E12 (2019).
	50	Comparison between MNI and Talairach Coordinates.	Lancaster, J. L. et al. Bias between MNI and Talairach coordinates analyzed using the ICBM-152 brain template. <i>Hum. Brain Mapp.</i> 28, 1194–1205 (2007).
	51	Original publication about functional parcellations.	Thomas Yeo, B. T. et al. The organization of the human cerebral cortex estimated by intrinsic functional connectivity. <i>Journal of Neurophysiology</i> 106, 1125–1165 (2011)
	52	Website from FreeSurfer.	https://surfer.nmr.mgh.harvard.edu/fswiki/CorticalParcellation_Yeo2011
	53	Thalamus - based on ex vivo analysis.	Iglesias, J. E. et al. A probabilistic atlas of the human thalamic nuclei combining ex vivo MRI and histology. <i>NeuroImage</i> 183, 314–326 (2018).
	54	Hippocampus - based on ex vivo analysis.	Iglesias, J. E. et al. A computational atlas of the hippocampal formation using ex vivo, ultra-high resolution MRI: Application to adaptive segmentation of in vivo MRI. <i>NeuroImage</i> 115, 117–137 (2015).
	55	Structural atlas of Cerebellum. Included with FSL.	Diedrichsen, J., Balsters, J. H., Flavell, J., Cussans, E. & Ramnani, N. A probabilistic MR atlas of the human cerebellum. <i>NeuroImage</i> 46, 39–46 (2009).
	56	Functional atlas of Cerebellum.	(1) Xue, A. et al. The Detailed Organization of the Human Cerebellum Estimated by Intrinsic Functional Connectivity Within the Individual. 69. (2) Buckner, R. L., Krienen, F. M., Castellanos, A., Diaz, J. C. & Yeo, B. T. T. The organization of the human cerebellum estimated by intrinsic functional connectivity. <i>Journal of Neurophysiology</i> 106, 2322–2345 (2011). (2) GitHub: https://github.com/ThomasYeoLab/CBIG/tree/master/stable_projects/brain_parcellation/Xue2021_IndCerebellum
	57	Pediatric/Neonatal.	Alexander, B. et al. A new neonatal cortical and subcortical brain atlas: the Melbourne Children's Regional Infant Brain (M-CRIB) atlas. <i>NeuroImage</i> 147, 841–851 (2017).
	58	Disease-specific: example of a multiple sclerosis lesional atlas.	Sahraian, M. A. & Radue, E.-W. <i>MRI atlas of MS lesions.</i> (Springer, 2008).